

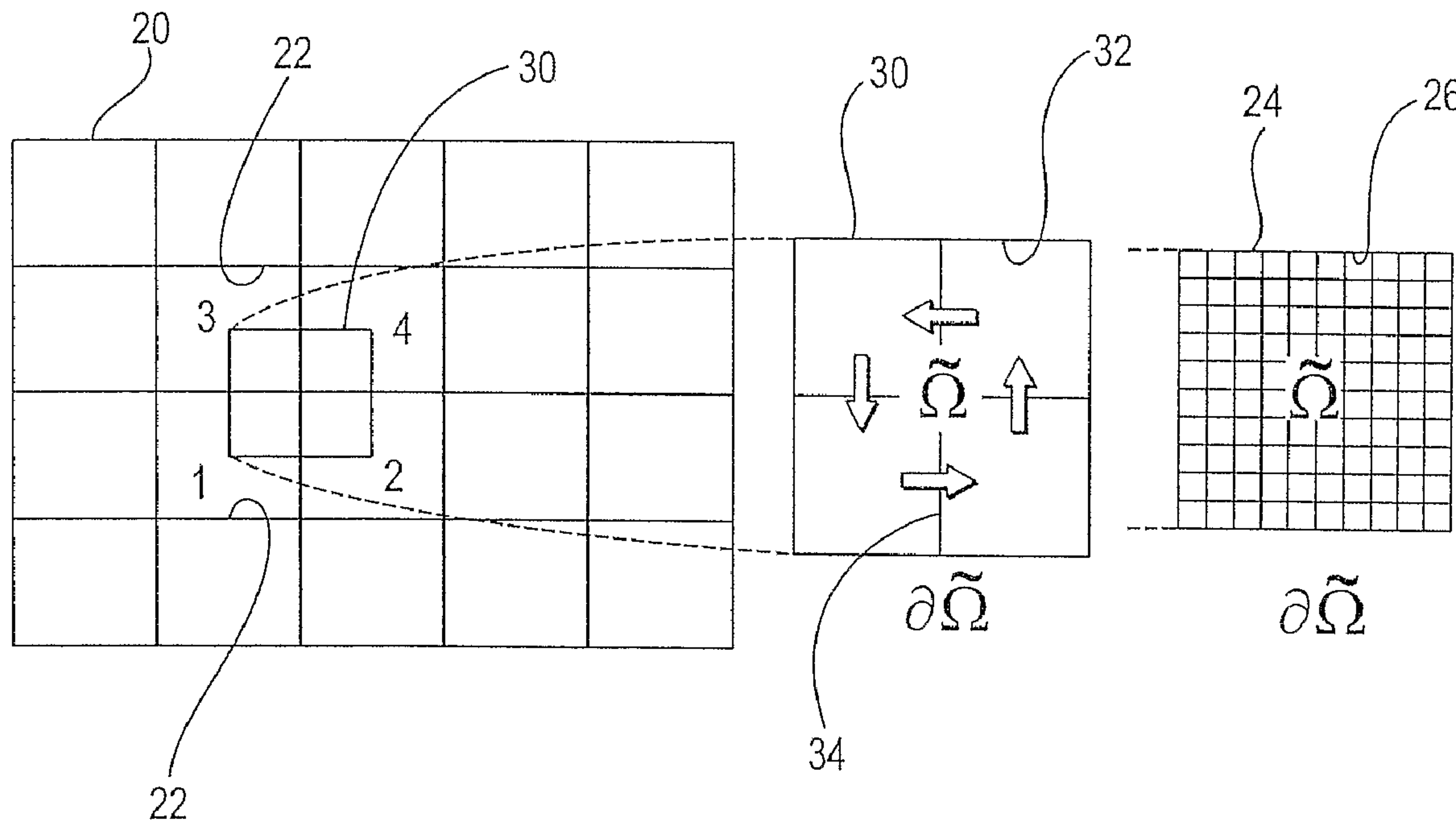


(86) Date de dépôt PCT/PCT Filing Date: 2005/11/21  
 (87) Date publication PCT/PCT Publication Date: 2006/06/01  
 (85) Entrée phase nationale/National Entry: 2007/05/22  
 (86) N° demande PCT/PCT Application No.: US 2005/042632  
 (87) N° publication PCT/PCT Publication No.: 2006/058171  
 (30) Priorité/Priority: 2004/11/23 (US10/997,539)

(51) Cl.Int./Int.Cl. *G06G 7/48* (2006.01)  
 (71) Demandeurs/Applicants:  
 CHEVRON U.S.A. INC., US;  
 SCHLUMBERGER TECHNOLOGY CORPORATION,  
 US;  
 SERVICES PETROLIERS SCHLUMBERGER, FR;  
 ETH ZURICH, CH  
 (72) Inventeurs/Inventors:  
 JENNY, PATRICK, CH;  
 LEE, SEONG, US;  
 TCHELEPI, HAMDIA A., US  
 (74) Agent: SIM & MCBURNEY

(54) Titre : PROCÉDE A VOLUME FINI ET ECHELLE MULTIPLE UTILISE POUR UNE SIMULATION D'ÉCOULEMENTS SOUTERRAINS

(54) Title: MULTI-SCALE FINITE-VOLUME METHOD FOR USE IN SUBSURFACE FLOW SIMULATION



(57) **Abrégé/Abstract:**

A multi-scale finite-volume (MSFV) method to solve elliptic problems with a plurality of spatial scales arising from single or multi-phase flows in porous media is provided. The method efficiently captures the effects of small scales on a coarse grid, is conservative, and treats tensor permeabilities correctly. The underlying idea is to construct transmissibilities that capture the local properties of a differential operator. This leads to a multi-point discretization scheme for a finite-volume solution algorithm. Transmissibilities for the MSFV method are preferably constructed only once as a preprocessing step and can be computed locally.

(12) INTERNATIONAL APPLICATION PUBLISHED UNDER THE PATENT COOPERATION TREATY (PCT)

(19) World Intellectual Property Organization  
International Bureau(43) International Publication Date  
1 June 2006 (01.06.2006)

PCT

(10) International Publication Number  
**WO 2006/058171 A2**

(51) International Patent Classification:

G06G 7/48 (2006.01)

(21) International Application Number:

PCT/US2005/042632

(22) International Filing Date:

21 November 2005 (21.11.2005)

(25) Filing Language:

English

(26) Publication Language:

English

(30) Priority Data:

10/997,539 23 November 2004 (23.11.2004) US

(71) Applicants (for all designated States except US):

**CHEVRON U.S.A. INC.** [US/US]; 6001 Bollinger Canyon Road, 3rd Floor, San Ramon, CA 94583 (US). **SCHLUMBERGER TECHNOLOGY CORPORATION** [US/US]; 5599 San Felipe, Suite 1700, Houston, Texas 77056 (US). **SERVICES PETROLIERS SCHLUMBERGER** [FR/FR]; 42, Rue Saint Dominique, F-75007 Paris (FR).

(71) Applicants (for US only):

**SCHLUMBERGER CANADA LIMITED** [CA/CA]; 2400, 801 6th Avenue S.w., Calgary, Alberta, T2P 3W2 (CA). **SCHLUMBERGER HOLDINGS LIMITED** [GB/GB]; P.O BOX 71, Craigmuir Chambers, Roadtown, Tortola (GB).

(71) Applicant (for all designated States except US):

**ETH ZURICH** [CH/CH]; Sonneggstr. 3, CH-8092 Zurich (CH).

(72) Inventors; and

(75) Inventors/Applicants (for US only):

**JENNY, Patrick** [CH/CH]; Ruetihofstrasse 42, CH-8049 Zurich (CH). **LEE, Seong** [US/US]; 6013 Christie Avenue, Emeryville, CA 94608 (US). **TCHELEPI, Hamdi, A.** [US/US]; 120 West 3rd Avenue, Apt. 710, San Mateo, CA 94402 (US).

(74) Agents:

**SCHULTE, Richard** et al.; CHEVRONTEX-ACO CORPORATION, LAW DEPARTMENT, Post Office Box 6006, San Ramon, CA 94583-0806 (US).

(81) Designated States (unless otherwise indicated, for every

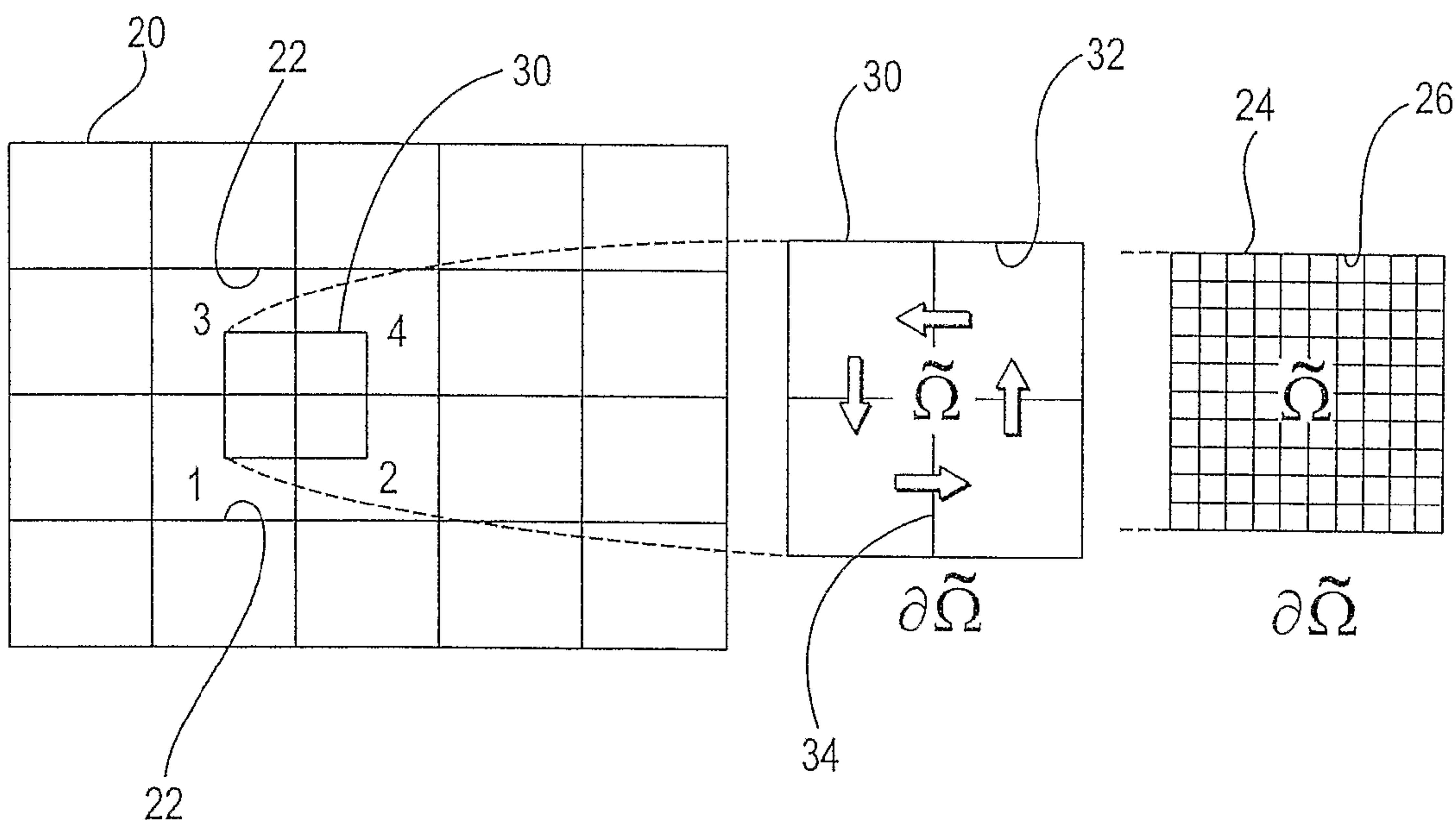
kind of national protection available): AE, AG, AL, AM, AT, AU, AZ, BA, BB, BG, BR, BW, BY, BZ, CA, CH, CN, CO, CR, CU, CZ, DE, DK, DM, DZ, EC, EE, EG, ES, FI, GB, GD, GE, GH, GM, HR, HU, ID, IL, IN, IS, JP, KE, KG, KM, KN, KP, KR, KZ, LC, LK, LR, LS, LT, LU, LV, LY, MA, MD, MG, MK, MN, MW, MX, MZ, NA, NG, NI, NO, NZ, OM, PG, PH, PL, PT, RO, RU, SC, SD, SE, SG, SK, SL, SM, SY, TJ, TM, TN, TR, TT, TZ, UA, UG, US, UZ, VC, VN, YU, ZA, ZM, ZW.

(84) Designated States (unless otherwise indicated, for every

kind of regional protection available): ARIPO (BW, GH,

[Continued on next page]

(54) Title: MULTI-SCALE FINITE-VOLUME METHOD FOR USE IN SUBSURFACE FLOW SIMULATION



(57) **Abstract:** A multi-scale finite-volume (MSFV) method to solve elliptic problems with a plurality of spatial scales arising from single or multi-phase flows in porous media is provided. The method efficiently captures the effects of small scales on a coarse grid, is conservative, and treats tensor permeabilities correctly. The underlying idea is to construct transmissibilities that capture the local properties of a differential operator. This leads to a multi-point discretization scheme for a finite-volume solution algorithm. Transmissibilities for the MSFV method are preferably constructed only once as a preprocessing step and can be computed locally.

WO 2006/058171 A2

**WO 2006/058171 A2**

GM, KE, LS, MW, MZ, NA, SD, SL, SZ, TZ, UG, ZM, ZW), Eurasian (AM, AZ, BY, KG, KZ, MD, RU, TJ, TM), European (AT, BE, BG, CH, CY, CZ, DE, DK, EE, ES, FI, FR, GB, GR, HU, IE, IS, IT, LT, LU, LV, MC, NL, PL, PT, RO, SE, SI, SK, TR), OAPI (BF, BJ, CF, CG, CI, CM, GA, GN, GQ, GW, ML, MR, NE, SN, TD, TG).

**Published:**

— *without international search report and to be republished upon receipt of that report*

*For two-letter codes and other abbreviations, refer to the "Guidance Notes on Codes and Abbreviations" appearing at the beginning of each regular issue of the PCT Gazette.*

1 MULTI-SCALE FINITE-VOLUME METHOD  
2 FOR USE IN SUBSURFACE FLOW SIMULATION

3  
4 RELATED APPLICATIONS

5  
6 This application is a continuation-in-part of co-pending U.S. Patent Application  
7 Serial No. 10/383,908, entitled "Multi-Scale Finite-Volume Method for Use in  
8 Subsurface Flow Simulation", filed on March 6, 2003 and is a  
9 continuation-in-part of co-pending application entitled "Multi-Scale  
10 Finite-Volume Method for Use in Subsurface Flow Simulation", filed on  
11 September 22, 2004, which is a continuation of co-pending U.S. Patent  
12 Application Serial No. 10/383,908, entitled "Multi-Scale Finite-Volume Method  
13 for Use in Subsurface Flow Simulation", filed on March 6, 2003.

14  
15 TECHNICAL FIELD

16  
17 The present invention relates generally to subsurface reservoir simulators,  
18 and more particularly, to those simulators which use multi-scale physics to  
19 simulate flow in an underground reservoir.

20  
21 BACKGROUND OF THE INVENTION

22  
23 The level of detail available in reservoir description often exceeds the  
24 computational capability of existing reservoir simulators. This resolution gap is  
25 usually tackled by upscaling the fine-scale description to sizes that can be  
26 treated by a full-featured simulator. In upscaling, the original model is  
27 coarsened using a computationally inexpensive process. In flow-based  
28 methods, the process is based on single-phase flow. A simulation study is  
29 then performed using the coarsened model. Upscaling methods such as these  
30 have proven to be quite successful. However, it is not possible to have a prior  
31 estimate of the errors that are present when complex flow processes are  
32 investigated using coarse models constructed via these simplified settings.

1 Various fundamentally different multi-scale approaches for flow in  
2 porous media have been proposed to accommodate the fine-scale  
3 description directly. As opposed to upscaling, the multi-scale approach  
4 targets the full problem with the original resolution. The upscaling  
5 methodology is typically based on resolving the length and time-scales  
6 of interest by maximizing local operations. Arbogast et al. (T. Arbogast,  
7 *Numerical subgrid upscaling of two phase flow in porous media*,  
8 Technical report, Texas Institute for Computational and Applied Mathematics,  
9 The University of Texas at Austin, 1999, and T. Arbogast and S.L. Bryant,  
10 *Numerical subgrid upscaling for waterflood simulations*, SPE 66375, 2001)  
11 presented a mixed finite-element method where fine-scale effects are  
12 localized by a boundary condition assumption at the coarse element  
13 boundaries. Then the small-scale influence is coupled with the coarse-scale  
14 effects by numerical Greens functions. Hou and Wu (T. Hou and X.H. Wu,  
15 *A multiscale finite element method for elliptic problems in composite materials*  
16 *and porous media*, J. Comp. Phys., 134:169-189, 1997) employed a  
17 finite-element approach and constructed specific basis functions which  
18 capture the small scales. Again, localization is achieved by boundary  
19 condition assumptions for the coarse elements. To reduce the effects of these  
20 boundary conditions, an oversampling technique can be applied. Chen and  
21 Hou (Z. Chen and T.Y. Hou, *A mixed finite element method for elliptic*  
22 *problems with rapidly oscillating coefficients*, Math. Comput., June 2002)  
23 utilized these ideas in combination with a mixed finite-element approach.  
24 Another approach by Beckie et al. (R. Beckie, A.A. Aldama, and E.F. Wood,  
25 *Modeling the large-scale dynamics of saturated groundwater flow using*  
26 *spatial filtering*, Water Resources Research, 32:1269-1280, 1996) is based on  
27 large eddy simulation (LES) techniques which are commonly used for  
28 turbulence modeling.  
29  
30 Lee et al. (S.H. Lee, L.J. Durlofsky, M.F. Lough, and W.H. Chen,  
31 *Finite difference simulation of geologically complex reservoirs with tensor*  
32 *permeabilities*, SPERE&E, pages 567-574, 1998) developed a flux-continuous

1 finite-difference (FCFD) scheme for 2D models. Lee et al. further developed a  
2 method to address 3D models (S.H. Lee, H. Tchelepi, P. Jenny and  
3 L. Dechant, *Implementation of a flux continuous finite-difference method for*  
4 *stratigraphic, hexahedron grids*, SPE Journal, September, pages 269-277,  
5 2002). Jenny et al. (P. Jenny, C. Wolfsteiner, S.H. Lee and L.J. Durlofsky,  
6 *Modeling flow in geometrically complex reservoirs using hexahedral*  
7 *multi-block grids*, SPE Journal, June, pages 149-157, 2002) later  
8 implemented this scheme in a multi-block simulator.

9  
10 In light of the above modeling efforts, there is a need for a simulation method  
11 which more efficiently captures the effects of small scales on a coarse grid.  
12 Ideally, the method would be conservative and also treat tensor permeabilities  
13 correctly. Further, preferably the reconstructed fine-scale solution would  
14 satisfy the proper mass balance on the fine-scale. The present invention  
15 provides such a simulation method.

#### 16 17 SUMMARY OF THE INVENTION

18  
19 A multi-scale finite-volume (MSFV) approach is taught for solving elliptic or  
20 parabolic problems such as those found in subsurface flow simulators.  
21 Advantages of the present MSFV method are that it fits nicely into a  
22 finite-volume framework, it allows for computing effective coarse-scale  
23 transmissibilities, treats tensor permeabilities properly, and is conservative at  
24 both the coarse and fine-scales. The present method is computationally  
25 efficient relative to reservoir simulation now in use and is well suited for  
26 massive parallel computation. The present invention can be applied to 3D  
27 unstructured grids and also to multi-phase flow. Further, the reconstructed  
28 fine-scale solution satisfies the proper mass balance on the fine-scale.  
29  
30 A multi-scale approach is described which results in effective transmissibilities  
31 for the coarse-scale problem. Once the transmissibilities are constructed, the  
32 MSFV method uses a finite-volume scheme employing multi-point stencils for

1 flux discretization. The approach is conservative and treats tensor  
2 permeabilities correctly. This method is easily applied using existing  
3 finite-volume codes, and once the transmissibilities are computed, the method  
4 is computationally very efficient. In computing the effective transmissibilities,  
5 closure assumptions are employed.

6  
7 A significant characteristic of the present multi-scale method is that two sets  
8 of basis functions are employed. A first set of dual basis functions is  
9 computed to construct transmissibilities between coarse cells. A second set of  
10 locally computed fine-scale basis functions is utilized to reconstruct a  
11 fine-scale velocity field from a coarse scale solution. This second set of  
12 fine-scale basis functions is designed such that the reconstructed fine-scale  
13 velocity solution is fully consistent with the transmissibilities. Further, the  
14 solution satisfies the proper mass balance on the small scale.

15  
16 The MSFV method may be used in modeling a subsurface reservoir. A fine  
17 grid is first created defining a plurality of fine cells. A permeability field and  
18 other fine-scale properties are associated with the fine cells. Next, a coarse  
19 grid is created which defines a plurality of coarse cells having interfaces  
20 between the coarse cells. The coarse cells are ideally aggregates of the fine  
21 cells. A dual coarse grid is constructed defining a plurality of dual coarse  
22 control volumes. The dual coarse control volumes are ideally also aggregates  
23 of the fine cells. Boundaries surround the dual coarse control volumes.

24  
25 Dual basis functions are then calculated on the dual coarse control volumes  
26 by solving local elliptic or parabolic problems, preferably using boundary  
27 conditions obtained from solving reduced problems along the interfaces of the  
28 coarse cells. Fluxes, preferably integral fluxes, are then extracted across the  
29 interfaces of the coarse cells from the dual basis functions. These fluxes are  
30 assembled to obtain effective transmissibilities between coarse cells of the  
31 coarse cell grid. The transmissibilities can be used for coarse scale finite  
32 volume calculations.

1 A fine-scale velocity field may be established. A finite volume method is used  
2 to calculate pressures in the coarse cells utilizing the transmissibilities  
3 between cells. Fine-scale basis functions are computed by solving local  
4 elliptic or parabolic flow problems on the coarse cells and by utilizing  
5 fine-scale fluxes across the interfaces of the coarse cells which are extracted  
6 from the dual basis functions. Finally, the fine-scale basis functions and the  
7 corresponding coarse cell pressures are combined to extract the fine-scale  
8 velocity field.

9  
10 A transport problem may be solved on the fine grid by using the fine-scale  
11 velocity field. Ideally, the transport problem is solved iteratively in two stages.  
12 In the first stage, a fine-scale velocity field is obtained from solving a pressure  
13 equation. In the second stage, the transport problem is solved on the fine cells  
14 using the fine-scale velocity field. A Schwartz overlap technique can be  
15 applied to solve the transport problem locally on each coarse cell with an  
16 implicit upwind scheme.

17  
18 A solution may be computed on the coarse cells at an incremental time and  
19 properties, such as a mobility coefficient, may be generated for the fine cells  
20 at the incremental time. If a predetermined condition is not met for all fine cells  
21 inside a dual coarse control volume, then the dual and fine-scale basis  
22 functions in that dual coarse control volume are reconstructed.

23

#### 24 BRIEF DESCRIPTION OF THE DRAWINGS

25

26 These and other objects, features and advantages of the present invention  
27 will become better understood with regard to the following description,  
28 pending claims and accompanying drawings where:

29

30 FIG. 1 illustrates a coarse 2D grid of coarse cells with an overlying dual  
31 coarse grid including a dual coarse control volume and an underlying fine grid  
32 of fine cells;



1 FIG. 2 illustrates a coarse grid including nine adjacent coarse cells (bold solid  
2 lines) with a corresponding overlying dual coarse grid (bold dashed lines)  
3 including dual coarse control volumes and an underlying fine grid (thin dotted  
4 lines) of fine cells;  
5  
6 FIG. 3 shows flux contribution  $q_A^{(2)}$  and  $q_B^{(2)}$  due to the pressure in a particular  
7 coarse cell 2;  
8 FIG. 4 is a flowchart describing the overall steps used in a preferred  
9 embodiment of a reservoir simulation which employs a multi-scale  
10 finite-volume (MSFV) method made in accordance with this invention;  
11  
12 FIG. 5 is a flowchart further detailing steps used to determine transmissibilities  
13 T between coarse cells;  
14  
15 FIG. 6 is a flow chart further describing steps used to construct a set of  
16 fine-scale basis functions and to extract a fine-scale velocity field;  
17  
18 FIG. 7 is a flowchart depicting coupling between pressure and the saturation  
19 equations which utilize an implicit solution scheme and wherein  $\Pi$  and  $\Sigma$  are  
20 operators used to update total velocity and saturation, respectively, during a  
21 single time step;  
22  
23 FIG. 8 is an illustration of the use of an adaptive scheme to selectively update  
24 basis functions;  
25  
26 FIG. 9 is an illustration of a permeability field associated with a SPE 10  
27 problem;  
28  
29 FIGS. 10A-B are illustrations of permeability fields of a top layer and a bottom  
30 layer of cells from the SPE 10 problem;

1 FIGS. 11A-B are illustrations of saturation fields of top layers of cells created  
 2 using the MSFV method and FIG. 11C is an illustration of a saturation field  
 3 computed by a conventional fine-scale reservoir simulator;

4

5 FIGS. 12A-B are illustrations of saturation fields of bottom layers of cells  
 6 created using the MSFV method and FIG. 12C is an illustration of a saturation  
 7 field computed by a conventional fine-scale reservoir computer;

8

9 FIGS. 13A-B are graphs of oil cut and oil recovery;

10

11 FIG. 14 is an illustration of a 3D test case having a grid of 10 x 22 x 17 grid  
 12 cells and including injector and producer wells; and

13

14 FIG. 15 is a graph of oil cut and oil recovery.

15

## 16 BEST MODES FOR CARRYING OUT THE INVENTION

17

### 18 I. FLOW PROBLEM

#### 19 A. *One Phase Flow*

20 Fluid flow in a porous media can be described by the elliptic problem:

$$21 \quad \nabla \cdot (\lambda \cdot \nabla p) = f \text{ on } \Omega \quad (1)$$

22 where  $p$  is the pressure,  $\lambda$  is the mobility coefficient (permeability,  $K$ , divided  
 23 by fluid viscosity,  $\mu$ ) and  $\Omega$  is a volume or region of a subsurface which is to  
 24 be simulated. A source term  $f$  represents wells, and in the compressible  
 25 case, time derivatives. Permeability heterogeneity is a dominant factor in  
 26 dictating the flow behavior in natural porous formations. The heterogeneity of  
 27 permeability  $K$  is usually represented as a complex multi-scale function of  
 28 space. Moreover, permeability  $K$  tends to be a highly discontinuous full tensor.  
 29 Resolving the spatial correlation structures and capturing the variability of  
 30 permeability requires a highly detailed reservoir description.

1 The velocity  $u$  of fluid flow is related to the pressure field through Darcy's law:

$$2 \quad u = -\lambda \cdot \nabla p. \quad (2)$$

3 On the boundary of a volume,  $\partial\Omega$ , the flux  $q = u \cdot \nu$  is specified, where  $\nu$  is the  
4 boundary unit normal vector pointing outward. Equations (1) and (2) describe  
5 incompressible flow in a porous media. These equations apply for both single  
6 and multi-phase flows when appropriate interpretations of the mobility  
7 coefficient  $\lambda$  and velocity  $u$  are made. This elliptic problem is a simple, yet  
8 representative, description of the type of systems that should be handled  
9 efficiently by a subsurface flow simulator. Moreover, the ability to handle this  
10 limiting case of incompressible flow ensures that compressible systems can  
11 be treated as a subset.

12

### 13 *B. Two Phase Flow*

14 The flow of two incompressible phases in a heterogeneous domain may be  
15 mathematically described by the following:

$$16 \quad \Phi \frac{\partial S_o}{\partial t} - \frac{\partial}{\partial x_i} \left( k \frac{k_{r_o}}{\mu_o} \frac{\partial p}{\partial x_i} \right) = -q_o$$

17 (3)

$$18 \quad \Phi \frac{\partial S_w}{\partial t} - \frac{\partial}{\partial x_i} \left( k \frac{k_{r_w}}{\mu_w} \frac{\partial p}{\partial x_i} \right) = -q_w$$

19 on a volume  $\Omega$ , where  $p$  is the pressure,  $S_{o,w}$  are the saturations (the  
20 subscripts  $o$  and  $w$  stand for oil and water, respectively) with  $0 \leq S_{o,w} \leq 1$  and  
21  $S_o + S_w \equiv 1$ ,  $k$  is the heterogeneous permeability,  $k_{r_{o,w}}$  are the relative  
22 permeabilities (which are functions of  $S_{o,w}$ ),  $\mu_{o,w}$  the viscosities and  $q_{o,w}$  are  
23 source terms which represent the wells. The system assumes that capillary  
24 pressure and gravity are negligible. Equivalently, system (3) can be written as:

$$25 \quad -\nabla \cdot u = q_o + q_w \quad (4)$$

$$26 \quad \Phi \frac{\partial S_o}{\partial t} + \nabla \cdot \left( \frac{k_o}{k_o + k_w} u \right) = -q_o \quad (5)$$

27 on  $\Omega$  with

1 
$$u = -\lambda \nabla p. \quad (6)$$

2 and the total mobility

3 
$$\lambda = k(k_o + k_w), \quad (7)$$

4 where  $k_j \equiv k_{rj} / \mu_j$  for  $j \in \{o, w\}$ .

5

6 Equation (4) is known as the "pressure equation" and equation (5) as the  
7 "hyperbolic transport equation." Again, equations (4) and (5) are a  
8 representative description of the type of systems that should be handled  
9 efficiently by a subsurface flow simulator. Such flow simulators, and  
10 techniques employed to simulate flow, are well known to those skilled in the  
11 art and are described in publications such as Petroleum Reservoir Simulation,  
12 K. Aziz and A. Settari, Stanford Bookstore Custom Publishing, 1999.

13

## 14 II. MULTI-SCALE FINITE-VOLUME (MSFV) METHOD

### 15 A. MSFV Method for One Phase Flow

#### 16 1. Finite-Volume Method

17 A cell centered finite-volume method will now be briefly described. To solve  
18 the problem of equation (1), the overall domain or volume  $\Omega$  is partitioned into  
19 smaller volumes  $\{\bar{\Omega}_i\}$ . A finite-volume solution then satisfies

20 
$$\int_{\bar{\Omega}_i} \nabla \cdot u \, d\Omega = \int_{\partial \bar{\Omega}_i} u \cdot \bar{\nu} \, d\Gamma = - \int_{\bar{\Omega}_i} f \, d\Omega \quad (8)$$

21 for each control volume  $\bar{\Omega}_i$ , where  $\bar{\nu}$  is the unit normal vector of the volume  
22 boundary  $\partial \bar{\Omega}_i$  pointing outward. The challenge is to find a good  
23 approximation for  $u \cdot \bar{\nu}$  at  $\partial \bar{\Omega}_i$ . In general, the flux is expressed as:

24 
$$u \cdot \bar{\nu} = \sum_{k=1}^n T^k \bar{p}^k. \quad (9)$$

25 Equation (9) is a linear combination of the pressure values,  $\bar{p}$ , in the volumes  
26  $\{\bar{\Omega}_i\}$  of the domain  $\Omega$ . The total number of volumes is  $n$  and  $T^k$  denotes  
27 transmissibility between volumes  $\{\bar{\Omega}_i\}$ . By definition, the fluxes of equation (9)

1 are continuous across the interfaces of the volumes  $\{\bar{\Omega}_i\}$  and, as a result, the  
 2 finite-volume method is conservative.

3

#### 4 2. Construction of the Effective Transmissibilities

5 The MSFV method results in multi-point stencils for coarse-scale fluxes. For  
 6 the following description, an orthogonal 2D grid 20 of grid cells 22 is used, as  
 7 shown in FIG. 1. An underlying fine grid 24 of fine grid cells 26 contains the  
 8 fine-scale permeability  $K$  information. To compute the transmissibilities  $T$   
 9 between coarse grid cells 22, a dual coarse grid 30 of dual coarse control  
 10 volumes 32 is used. A control volume 32 of the dual grid 30,  $\tilde{\Omega}$ , is constructed  
 11 by connecting the mid-points of four adjacent coarse grid cells 22. To relate  
 12 the fluxes across the coarse grid cell interfaces 34 which lie inside a particular  
 13 control volume 32, or  $\tilde{\Omega}$ , to the finite-volume pressures  $\bar{p}^k (k=1,4)$  in the four  
 14 adjacent coarse grid cells 22, a local elliptical problem in the preferred  
 15 embodiment is defined as

$$16 \quad \nabla \cdot (\lambda \cdot \nabla p) = 0 \text{ on } \tilde{\Omega}. \quad (10)$$

17 For one skilled in the art, the method can easily be adapted to use a local  
 18 parabolic problem.

19

20 For an elliptic problem, Dirichlet or Neumann boundary conditions are to be  
 21 specified on boundary  $\partial\tilde{\Omega}$ . Ideally, the imposed boundary conditions should  
 22 approximate the true flow conditions experienced by the sub-domain in the full  
 23 system. These boundary conditions can be time and flow dependent. Since  
 24 the sub-domain is embedded in the whole system, Wallstrom et al.  
 25 (T.C. Wallstrom, T.Y. Hou, M.A. Christie, L.J. Durlofsky, and D.H. Sharp,  
 26 *Application of a new two-phase upscaling technique to realistic reservoir cross*  
 27 *sections*, SPE 51939, presented at the SPE Symposium on Reservoir  
 28 Simulation, Houston, 1999) found that a constant pressure condition at the  
 29 sub-domain boundary tends to overestimate flow contributions from high  
 30 permeability areas. If the correlation length of permeability is not much larger  
 31 than the grid size, the flow contribution from high permeability areas is not

1 proportional to the nominal permeability ratio. The transmissibility between  
 2 two cells is a harmonic mean that is closer to the lower permeability. As a  
 3 result, uniform flux conditions along the boundary often yield much better  
 4 numerical results for a sub-domain problem than linear or constant pressure  
 5 conditions.

6

7 Hou and Wu (T. Hou and W.H. Wu, *A multiscale finite element method for*  
 8 *elliptic problems in composite materials and porous media*, J. Comp. Phys,  
 9 134:169-189, 1997) also proposed solving a reduced problem

$$10 \quad \frac{\partial}{\partial x_t} \left( \lambda_{ij} \frac{\partial p}{\partial x_j} \right)_t = 0, \quad (11)$$

11 to specify the boundary conditions for the local problem. The subscript  $t$   
 12 denotes the component parallel to the boundary of the dual coarse control  
 13 volume  $\tilde{\Omega}$  or  $\partial\tilde{\Omega}$ . For equation (11) and for the following part of this  
 14 specification, Einstein summation convention will be used. The elliptic  
 15 problem on a control volume  $\tilde{\Omega}$  with boundary conditions of equation (11) on  
 16  $\partial\tilde{\Omega}$  can be solved by any appropriate numerical method. In order to obtain a  
 17 pressure solution that depends linearly on the pressures  $\bar{p}^k (j=1,4)$ , this  
 18 preferred embodiment solves four elliptic problems, one for each cell-center  
 19 pressure. For instance, to get the solution for the pressure  $\bar{p}^1$  in the coarse  
 20 grid cell having node 1 at its center,  $\bar{p}^k = \delta_{1k}$  is set. The four solutions provide  
 21 the dual basis functions  $\tilde{\Phi}^k (k=1,4)$  in control volume  $\tilde{\Omega}$ , and the pressure  
 22 solution of the local elliptic problem in a control volume  $\tilde{\Omega}$  is the linear  
 23 combination

$$24 \quad p = \sum_{k=1}^4 \bar{p}^k \tilde{\Phi}^k. \quad (12)$$

25 Accordingly, the flux  $q$  across the grid cell interfaces can be written as a  
 26 linear combination

$$1 \quad q = \sum_{k=1}^4 \bar{p}^k q^k, \quad (13)$$

2 where  $q^k (k=1,4)$  are the flux contributions from the corresponding dual basis  
 3 functions, given all  $\tilde{\Phi}^k (k=1,4)$  from all control volumes  $\tilde{\Omega}$ . The effective  
 4 transmissibilities  $T$  are computed, which can be used for finite-volume  
 5 simulations, by assembling the flux contributions, in the preferred embodiment  
 6 integral flux contributions across the cell interfaces 34.

7  
 8 Note that the domain  $\tilde{\Omega}$  can have any fine-scale distribution of mobility  
 9 coefficients  $\lambda$ . Of course the boundary condition given by equation (11) is an  
 10 approximation that allows one to decouple the local problems. The MSFV and  
 11 global fine-scale solutions are identical, only if equation (11) happens to  
 12 capture the exact fine-scale pressure solution. However, numerical  
 13 experiments have been performed which indicate that equation (11) is an  
 14 excellent approximation of the boundary condition.

15  
 16 Although the MSFV approach is a finite-volume method, it resembles the  
 17 multi-scale finite-element method of Wu and Hou, briefly mentioned above.  
 18 The construction of the dual basis functions is similar, though in the present  
 19 MSFV method they are represented on the dual coarse grid rather than on the  
 20 boundary of a finite element. A significant difference is that the present MSFV  
 21 method is a cell-centered finite-volume method and is conservative. On the  
 22 other hand, the mass matrix in the multi-scale finite-element method is  
 23 constructed based on a variational principle and does not ensure local  
 24 conservation. In the next section, the importance is illustrated of a fine-scale  
 25 velocity field that is conservative.

### 26 27 3. Reconstruction of a Conservative Fine-Scale Velocity Field

28 Fluxes across the coarse cell interfaces 34 can be accurately computed by  
 29 multi-scale transmissibilities  $T$ . In some cases, it is interesting to accurately  
 30 represent the small-scale velocities  $u$  (e.g., to predict the distribution of solute

1 transported by a fluid). A straightforward approach might appear to be to use  
2 the dual basis functions  $\tilde{\Phi}$  of equation (12). However, then the reconstructed  
3 fine-scale velocity field is, in general, discontinuous at the cell interfaces of the  
4 dual grid 30. Therefore, large errors can occur in the divergence field, and  
5 local mass balance is violated. Note that mass conservation is always  
6 satisfied for the coarse solution using the present MSFV method.

7

8 The construction of a second set of local fine-scale basis functions  $\Phi$  will now  
9 be described which is fully consistent with the fluxes  $q$  across the cell  
10 interfaces given by the dual basis functions  $\tilde{\Phi}$ . This second set of fine-scale  
11 basis functions  $\Phi$  allows a conservative fine-scale velocity field to be  
12 reconstructed.

13

14 FIG. 2 shows a coarse grid 20 with nine adjacent grid cells 22 and a  
15 corresponding dual grid 30 of dual coarse control volumes 32 or  $\tilde{\Omega}$ . For  
16 indexing purposes, these particular cells and corresponding dual volumes  
17 shall now be identified with numerals "1-9" and letters "A-D" at their respective  
18 centers. Also shown is the underlying fine grid 24 of fine grid cells 26. The  
19 coarse grid, having the nine adjacent coarse cells 1-9, is shown in bold solid  
20 lines. The corresponding dual grid 30 of dual coarse control volumes A-D are  
21 depicted with bold dashed lines. The underlying fine grid 24 of fine grid cells  
22 26 is shown with thin dotted lines.

23

24 To explain the reconstruction of the fine-scale velocity, the mass balance of  
25 the center grid cell 5 is examined. The coarse scale pressure solution,  
26 together with the dual basis functions  $\tilde{\Phi}$ , provides the fine-scale fluxes  $q$   
27 across the interfaces of coarse cell 5.

28

29 To obtain a proper representation of the fine-scale velocity field in coarse  
30 cell 5, (i) the fine-scale fluxes across an interface of coarse cell 5 must match,  
31 and (ii) the divergence of the fine-scale velocity field within the coarse volume  
32 satisfies



$$1 \quad \nabla \cdot \mathbf{u} = \frac{\int_{\partial \bar{\Omega}_5} q d\Gamma}{\int_{\bar{\Omega}_5} d\Omega}, \quad (14)$$

2 where  $\bar{\Omega}_5$  is the coarse grid cell 5. The fine-scale flux  $q$  across the boundary  
 3 of grid cell 5 depends on the coarse pressure solutions in grid cells 1-9.  
 4 Therefore, the fine-scale velocity field within coarse grid cell 5 can be  
 5 expressed as a superposition of fine-scale basis functions  $\Phi^i$  ( $i = 1,9$ ). With  
 6 the help of FIG. 3, which depicts the needed dual coarse control volumes, the  
 7 needed dual coarse control volumes, the construction the needed dual coarse  
 8 control volumes, the construction of the fine-scale the needed dual coarse  
 9 control volumes, the construction of the fine-scale the needed dual coarse  
 10 control volumes, the construction of the fine-scale the needed dual coarse  
 11 fine-scale basis functions  $\Phi^i$  will be described. Each coarse cell pressure  
 12  $\bar{p}(i=1,9)$  contributes to the fine-scale flux  $q$ . For example, let the contribution  
 13 of the pressure in cell 2 to the flux  $q$  in grid cell 5 be  $q^{(2)}$ . Note that  $q^{(2)}$  is  
 14 composed of contributions  $q_A^{(2)}$  and  $q_B^{(2)}$  coming from the dual basis functions  
 15 associated with node 2 of volume A and volume B, respectively. To compute  
 16 the fine-scale basis function  $\Phi^i$  associated with the pressure in a coarse cell  
 17  $i$ ,  $\bar{p}^j = \delta_{ij}$  is set, and the pressure field is constructed according to the  
 18 following equation.

$$19 \quad p = \sum_{k \in \{A,B,C,D\}} \sum_{j=1}^9 \bar{p}^j \tilde{\Phi}_k^j. \quad (15)$$

20 The fine-scale fluxes  $q$  are computed from the pressure field. These fluxes  
 21 provide the proper boundary condition for computing the fine-scale basis  
 22 function  $\Phi^i$ . To solve the elliptic problem

$$23 \quad \nabla \cdot (\lambda \cdot \nabla p) = f' \text{ on } \bar{\Omega}_5 \quad (16)$$

1 with the boundary conditions described above, solvability must be ensured.  
 2 This is achieved by setting

$$3 \quad f' = \frac{\int_{\partial\bar{\Omega}_5} q d\Gamma}{\int_{\bar{\Omega}_5} d\Omega}, \quad (17)$$

4 which is an equally distributed source term within  $\bar{\Omega}_5$ . Finally, the solution of  
 5 the elliptic problem, (16) and (17), is the fine-scale basis function  $\Phi^i$  for  
 6 coarse cell 5 associated with the pressure in volume  $i$ . The small-scale  
 7 velocity field is extracted from the superposition

$$8 \quad p = \sum_{j=1}^9 \bar{p}^j \Phi_5^j. \quad (18)$$

9 For incompressible flow, this velocity field is divergence free everywhere.  
 10 Computing the fine-scale basis functions  $\Phi^i$  requires solving nine small  
 11 elliptic problems, which are of the same size as those for the transmissibility  
 12 calculations. Note that this step is a preprocessing step and has to be done  
 13 only once. Furthermore, the construction of the fine-scale basis functions  
 14  $\Phi^i$  is independent and therefore well suited for parallel computation. The  
 15 reconstruction of the fine-scale velocity field is a simple superposition and is  
 16 ideally performed only in regions of interest.  
 17  
 18 Alternatively, a conservative fine-scale velocity field may also be constructed  
 19 directly in place. This construction may be performed as follows: (i) compute  
 20 the fine-scale fluxes across the coarse cell interfaces using the dual basis  
 21 functions with the pressures for the coarse cells; (ii) solve a pressure equation  
 22 on each of the coarse cells using the fine-scale fluxes computed in step (i) as  
 23 boundary conditions to obtain fine-scale pressures; (iii) compute the fine-scale  
 24 velocity field from Darcy's law using the fine-scale pressures obtained in step  
 25 (ii) with the underlying fine-scale permeability. The pressure solution of step  
 26 (ii) may be performed on a system with larger support (e.g., by over-sampling  
 27 around the coarse cell).

1     **III.     IMPLEMENTATION OF THE MSFV METHOD**

2     FIG. 4 is a flow chart summarizing the steps employed in a preferred  
3     embodiment in simulating a reservoir using the MSFV algorithm of this  
4     invention. The MSFV algorithm consists of six major steps:

5

6     A.     compute transmissibilities  $T$  for coarse-scale fluxes (step 100);

7

8     B.     construct fine-scale basis functions (step 200);

9

10    C.     compute a coarse solution at a new time level; (step 300);

11

12    D.     reconstructs the fine-scale velocity field in regions of interest  
13           (step 400);

14

15    E.     solve transport equations (step 500); and

16

17    F.     recomputes transmissibilities and also the fine-scale basis functions in  
18           regions where the total mobility has changed more than a  
19           predetermined amount (step 600).

20

21    Steps A-D describes a two-scale approach. The methodology can be applied  
22    recursively with successive levels of coarsening. In cases of extremely fine  
23    resolution, this multi-level approach should yield scalable solutions. Parts E  
24    and F account for transport and mobility changes due to evolving phases and  
25    will be described in more detail below.

26

27    A.     *Computing Transmissibilities for Coarse-Scale Fluxes – Step 100*

28    The transmissibility calculations can be done in a stand alone module  
29    (T-module) and are well suited for parallel computation. The transmissibilities  
30     $T$  can be written to a file for use by any finite-volume simulator that can handle  
31    multi-point flux discretization.

1 Referring now to FIG. 5, a flowchart describes the individual steps which are  
2 undertaken to compute the transmissibilities  $T$  for a coarse scale model. First,  
3 a fine-scale grid having fine cells with an associated permeability field  $K$  are  
4 created (step 110). Next, a coarse grid, having coarse cells corresponding to  
5 the fine-scale grid, is created (step 120). The fine and coarse grids are then  
6 passed into a transmissibility or  $T$ -module.

7 Dual coarse control volumes  $\tilde{\Omega}$  are constructed (step 130), one for each node  
8 of the coarse grid. For each dual coarse control volume  $\tilde{\Omega}$ , dual or coarse  
9 scale basis functions  $\Phi_{CS}$  are constructed (step 140) by solving local elliptic  
10 problems (equation (10)) for each volume  $\tilde{\Omega}$ . This local elliptic problem, as  
11 described in section II.A.2 above, and the permeability field  $K$  associated with  
12 the fine grid are used and the boundary conditions corresponding to equation  
13 (11) are utilized (step 135) in solving the elliptic problem. In cases where the  
14 fine and coarse grids are nonconforming (e.g., if unstructured grids are used),  
15 oversampling may be applied. Finally, the integral coarse scale fluxes  
16  $q$  across the interfaces of the coarse cells are extracted (step 150) from the  
17 dual basis functions  $\tilde{\Phi}$ . These integral coarse scale fluxes  $q$  are then  
18 assembled (step 160) to obtain MSFV-transmissibilities  $T$  between grid cells  
19 of the coarse grid.

20

21 The computation of transmissibilities  $T$  can be viewed as an upscaling  
22 procedure. That is, the constructed coarse pressure solutions are designed to  
23 account for, in some manner, the fine-scale description of the permeability  $K$   
24 in the original fine-scale grid model. Thus, part A – step 100 - computing  
25 transmissibilities, is preferably a separate preprocessing step used to coarsen  
26 the original fine-scale model to a size manageable by a conventional reservoir  
27 simulator.

28

29 These transmissibilities  $T$  may be written to a file for later use. A finite-volume  
30 simulator that can handle multi-point flux discretization can then use these  
31 transmissibilities  $T$ .

1 *B. Construction of Fine-Scale Basis Function and Fine-scale Velocity*  
2 *Field– Step 200*

3 FIG. 6 is a flowchart describing the steps taken to construct a set of fine-scale  
4 basis functions  $\Phi$  which can be isolated in a separate fine-scale basis  
5 function  $\Phi$  module. These fine-scale basis functions  $\Phi$  can then be used to  
6 create a fine-scale velocity field. This module is only necessary if there is an  
7 interest in reconstructing the fine-scale velocity field from the coarse pressure  
8 solution. As described in Section II.A.3 above, if the original dual basis  
9 functions  $\tilde{\Phi}$  are used in reconstructing the fine-scale velocity field, large mass  
10 balance errors can occur. Here, steps are described to compute the fine-scale  
11 basis functions  $\Phi$ , which can be used to reconstruct a conservative fine-scale  
12 velocity field. The procedure (step 200) of FIG. 4 follows the description of  
13 Section II.A.3 and has to be performed only once at the beginning of a  
14 simulation and is well suited for parallel computation.

15  
16 The fine-scale grid (step 210), with its corresponding permeability field  $K$ , the  
17 coarse grid (step 220), and the dual basis functions  $\tilde{\Phi}$  (step 230) are passed  
18 into a fine-scale basis function  $\Phi$ . A pressure field is constructed from the  
19 coarse scale pressure solution and dual basis functions (step 250). The fine-  
20 scale fluxes for the coarse cells are then computed (step 260). For each  
21 control volume, elliptic problems are solved, using the fine-scale fluxes as  
22 boundary conditions, to determine fine-scale basis functions (step 270). The  
23 fine-scale velocity field can then be computed from the superposition of cell  
24 pressures and fine-scale basis functions. The results may then be output from  
25 the module. Alternatively, the fine-scale velocity field can be computed directly  
26 in place as has been described above in section II.A.3. In many cases, the  
27 fine-scale velocity field has to be reconstructed in certain regions only, as will  
28 be described in fuller detail below. Therefore, in order to save memory and  
29 computing time, one can think of an in situ computation of the fine-scale basis  
30 functions  $\Phi$ , which, once computed, can be reused.

1 C. *Computation of the Coarse Solution at the New Time – Step 300*

2 Step 300 can be performed by virtually any multi-point stencil finite-volume  
3 code by using the MSFV-transmissibilities  $T$  for the flux calculation. These  
4 coarse fluxes effectively capture the large-scale behavior of the solution  
5 without resolving the small scales.

6

7 D. *Reconstruction of the Fine-Scale Velocity Field – Step 400*

8 Step 400 is straight forward. Reconstruction of the fine-scale velocity field in  
9 regions of interest is achieved by superposition of the fine-scale basis FIG. 6.  
10 Alternatively, the fine-scale velocity field can be computed directly in functions  
11  $\Phi^i$  as described in section II.A.3, step B above and as shown in place as  
12 described above in section II.A.3. Of course, many variations of the MSFV  
13 method can be devised. It may be advantageous; however, that construction  
14 of the transmissibilities  $T$  and fine-scale basis functions  $\Phi$  can be done in  
15 modules separate from the simulator.

16

17 E. *Solving Pressure and Transport Equations*

18 1. Numerical solution algorithm – explicit solution

19 Multi-phase flow problems may be solved in two stages. First, the total  
20 velocity field is obtained from solving the pressure equation (4), and then the  
21 hyperbolic transport equation (5) is solved. To solve the pressure equation,  
22 the MSFV method, which has been described above is used. The difference  
23 from single phase flow is that in this case the mobility term  $\lambda$  reflects the total  
24 mobility of both phases, and then the obtained velocity field  $u$  is the total  
25 velocity in the domain. The reconstructed fine-scale velocity field  $u$  is then  
26 used to solve the transport equation on the fine grid. The values of  $k_{o,w}$  are  
27 taken from the upwind direction; time integration may be obtained using a  
28 backward Euler scheme. Note that, in general, the dual and fine-scale basis  
29 functions  $(\tilde{\Phi}, \Phi)$  must be recomputed each time step due to changes in the  
30 saturation (mobility) field.

1 2. Numerical Solution Algorithm - Implicit Coupling

2 In the preferred embodiment of this invention, the MSFV method utilizes an  
3 algorithm with implicit calculations. The multi-phase flow problem is solved  
4 iteratively in two stages. See FIG. 7 for a diagram of this method illustrating  
5 the coupling between the pressure and saturation equations.

6

7 First, in each Newton step, a saturation field  $S$  is established – either initial  
8 input or through iteration (step 510). Next, a pressure equation (see equation  
9 (19) below) is solved (step 520) using the MSFV techniques described above  
10 to obtain (step 530) the total velocity field. Then a transport equation (see  
11 equation (20) below) is solved (step 540) on the fine grid by using the  
12 reconstructed fine-scale velocity field  $u$ . In this solution, a Schwarz overlap  
13 technique is applied, i.e., the transport problem is solved locally on each  
14 coarse volume with an implicit upwind scheme, where the saturation values  
15 from the neighboring coarse volumes at the previous iteration level are used  
16 for the boundary conditions. Once the Schwarz overlap scheme has  
17 converged (steps 550, 560) — for hyperbolic systems this method is very  
18 efficient — the new saturation distribution determines the new total mobility  
19 field for the pressure problem of the next Newton iteration. Note that, in  
20 general, some of the basis functions have to be recomputed each iteration.

21

22 The superscripts  $n$  and  $\nu$  denote the old time and iteration levels,  
23 respectively. Saturation is represented by  $S$ , the total velocity field by  $u$ , the  
24 computation of the velocity by the operator  $\Pi$ , and the computation of the  
25 saturation by  $\Sigma$ . The new pressure field  $p^{\nu+1}$  is obtained by solving

26 
$$\nabla \cdot \left( k \left( k_o \left( S^\nu \right) + k_w \left( S^\nu \right) \right) \nabla p^{\nu+1} \right) = q_o + q_w, \quad (19)$$

27 from which the new velocity field  $u^{\nu+1}$  is computed. The new saturation field  
28  $S^{\nu+1}$  is obtained by solving

$$1 \quad \Phi \frac{S^{v+1} - S^n}{\Delta t} + \nabla \cdot \left( \frac{k_o(S^{v+1})}{k_o(S^{v+1}) + k_w(S^{v+1})} u^{v+1} \right) = -q_o \quad (20)$$

2 *F. Recomputing Transmissibilities and Fine-Scale Basis Functions –*  
 3 *Adaptive Scheme*

4 The most expensive part of the MSFV algorithm for multi-phase flow is the  
 5 reconstruction of the coarse scale and fine-scale basis functions ( $\tilde{\Phi}, \Phi$ ).

6 Therefore, to obtain higher efficiency, it is desirable to recompute the basis  
 7 functions only where it is absolutely necessary. An adaptive scheme can be  
 8 used to update these basis functions. In the preferred exemplary embodiment,  
 9 if the condition

$$10 \quad \frac{1}{1 + \varepsilon_\lambda} < \frac{\lambda^n}{\lambda^{n-1}} < 1 + \varepsilon_\lambda \quad (23)$$

11 is not fulfilled (the superscripts  $n$  and  $n-1$  denote the previous two time steps  
 12 and  $\varepsilon_\lambda$  is a defined value) for all fine cells inside a coarse dual volume, then  
 13 the dual basis functions of that control volume have to be reconstructed. Note  
 14 that condition (23) is true if  $\lambda$  changes by a factor which is larger than  
 15  $1/(1 + \varepsilon_\lambda)$  and smaller than  $1 + \varepsilon_\lambda$ . An illustration of this scheme is shown in  
 16 FIG. 8, where the fine and the coarse grid cells are drawn with thin and bold  
 17 lines, respectively. The black squares represent the fine cells in which  
 18 condition (23) is not fulfilled. The squares with bold dashed lines are the  
 19 control volumes for which the dual basis functions have to be reconstructed.  
 20 The shaded regions represent the coarse cells for which the fine-scale basis  
 21 functions have to be updated. In the schematic 2D example of FIG. 8, only 20  
 22 of 196 total dual basis functions and 117 of 324 total fine-scale basis functions  
 23 have to be reconstructed. Of course, these numbers depend heavily on the  
 24 defined threshold  $\varepsilon_\lambda$ . In general, a smaller threshold triggers more fine  
 25 volumes, and as a consequence more basis functions are recomputed each  
 26 time step. For a wide variety of test cases, it has been found that taking  $\varepsilon_\lambda$  to  
 27 be  $< 0.2$  yields marginal changes in the obtained results.



#### 1 IV. NUMERICAL RESULTS

2 This MSFV method, combined the implicit coupling scheme shown in FIG. 7,  
3 has been tested for two phase flow ( $\mu_o/\mu_w \equiv 10$ ) in a stiff 3D model with  
4 more than 140,000 fine cells. It has been demonstrated that the multi-scale  
5 results are in excellent agreement with the fine-scale solution. Moreover, the  
6 MSFV method has proven to be approximately 27 times more efficient than  
7 the established oil reservoir simulator Cheers. However, in many cases the  
8 computational efficiency is compromised due to the time step size restrictions  
9 inherent for IMPES schemes. This problem may be resolved by applying the  
10 fully implicit MSFV method, which was described in the previous section. Here  
11 numerical studies show the following:

12  
13 (1) The results obtained with the implicit MSFV method are in excellent  
14 agreement with the fine-scale results.

15

16 (2) The results obtained with the implicit MSFV method are not very  
17 sensitive to the choice of the coarse grid.

18

19 (3) The implicit MSFV for two phase flow overcomes the time step size  
20 restriction and therefore very large time steps can be applied.

21

22 (4) The results obtained with the implicit MSFV method are, to a large  
23 extent, insensitive to the time step size.

24

25 (5) The implicit MSFV method is very efficient.

26

27 For the fine-scale comparison runs, the established reservoir simulator  
28 Cheers was used. The efficiency of both the implicit MSFV method and the  
29 fine-scale reservoir simulator depends on the choice of various parameter  
30 settings which were not fully optimized.

1    A.     *Test Case*

2    To study the accuracy and efficiency of the fully implicit MSFV algorithm,  
3    2D and 3D test cases with uniformly spaced orthogonal 60 x 220 and  
4    60 x 220 x 85 grids were used. The 3D grid and permeability field are the  
5    same as for the SPE 10 test case, which is regarded as being extremely  
6    difficult for reservoir simulators. While this 3D test case is used for  
7    computational efficiency assessment, the 2D test cases, which consist of top  
8    and bottom layers, serves to study the accuracy of the MSFV method. FIG. 9  
9    illustrates the 3D test case posed by the permeability field of the SPE 10  
10   problem. The darker areas indicate lower permeability. An injector well is  
11   placed in the center of the field and four producers in the corners. These well  
12   locations are used for all of the following studies. The reservoir is initially filled  
13   with oil and  $\mu_o / \mu_w = 10$  and  $k_{r_{o,w}} = S_{o,w}^2$ .

14

15    B.     *2D Simulation of the Top and Bottom Layers*

16    The MSFV simulator used lacked a sophisticated well model. That is, wells  
17    are modeled by defining the total rates for each perforated coarse volume.  
18    Therefore, in order to make accuracy comparisons between MSFV and  
19    fine-scale (Chears reservoir simulator) results, each fine-scale volume inside  
20    each perforated coarse volume becomes a well in the Chears runs. For large  
21    3D models, this poses a technical problem since Chears reservoir simulator is  
22    not designed to handle an arbitrary large number of individual wells. For this  
23    reason, it was determined to do an accuracy assessment in 2D, i.e., with the  
24    top and the bottom layers of the 3D model. These two layers, for which the  
25    permeability fields are shown in FIGS. 10A and 10B, are representative for  
26    the two characteristically different regions of the full model.

27

28    MSFV simulations were performed with uniformly spaced 10 x 22 and  
29    20 x 44 coarse grids. The results were compared with the fine-scale solution  
30    on a 60 x 220 grid. As in the full 3D test case, there are four producers at the  
31    corners which are distributed over an area of 6 x 10 fine-scale volumes. The  
32    injector is located in the center of the domain and is distributed over an area

1 of 12 x 12 fine-scale volumes. The rates are the same for all fine-scale  
2 volumes (positive for the producer volumes and negative for the injector  
3 volumes). FIGS. 11A-C and 12A-C show the permeability fields of the  
4 respective top and the bottom layers. The black is indicative of low  
5 permeability. These two layers are representative for the two characteristically  
6 different regions of the full 3D model. FIGS. 11A-C and 12A-C show the  
7 computed saturation fields after 0.0933 PVI (pore volume injected) for the top  
8 and the bottom layers, respectively. While FIGS. 11C and 12C show the  
9 fine-scale reference solutions, FIGS 11A and 11B and 12A and 12B show the  
10 MSFV results for 10 x 22 and 20 x 44 coarse grids, respectively. For both  
11 layers, it can be observed that the agreement is excellent and that the  
12 multi-scale method is hardly sensitive to the choice of the coarse grid. A more  
13 quantitative comparison is shown in FIGS. 13A and 13B where the fine-scale  
14 and multi-scale oil cut and oil recovery curves are plotted. Considering the  
15 difficulty of these test problems and the fact that two independently  
16 implemented simulators are used for the comparisons, this agreement is quite  
17 good. In the following studies, it will be demonstrated that for a model with  
18 1,122,000 cells, the MSFV method is significantly more efficient than  
19 fine-scale simulations and the results remain accurate for very large time  
20 steps.

21

### 22 C. 3D Simulations

23 While 2D studies are appropriate to study the accuracy of the implicit MSFV  
24 method, large and stiff 3D computations are required for a meaningful  
25 efficiency assessment. A 3D test case was employed as described above. A  
26 coarse 10 x 22 x 17 grid, shown in FIG.14, was used and 0.5 pore volumes  
27 were injected. Opposed to the MSFV runs, the wells for the CHEARS  
28 simulations were defined on the fine-scale. Table 1 below shows CPU time  
29 and required number of times steps for the CHEARS simulation and two  
30 MSFV runs.

**TABLE 1**

Efficiency Comparison Between Msfv And Fine-Scale Simulations

| Simulator | CPU TIME<br>(minutes) | Time<br>steps | Recomputed Basis<br>Functions (%) | Coarse Pressure<br>Computations (%) |
|-----------|-----------------------|---------------|-----------------------------------|-------------------------------------|
| Chears    | 3325                  | 790           |                                   |                                     |
| MSFV      | 297                   | 200           | 10                                | 98                                  |
| MSFV      | 123                   | 50            | 26                                | 100                                 |

While Chears uses a control algorithm, the time step size in the multi-scale simulations was fixed. It is due to the size and stiffness of the problem that much smaller time steps have to be applied for a successful Chears simulation. The table shows that the implicit MSFV method can compute the solution approximately 27 times faster than CHEARS. FIG. 15 shows the oil cut and recovery curves obtained with multi-scale simulations using 50 and 200 time steps. The close agreement between the results confirms that the method is very robust in respect to time step size. Since the cost for MSFV simulation scales almost linearly with the problem size and since the dual and fine-scale basis function can be computed independently, the method is ideally suited for massive parallel computations and huge problems.

While in the foregoing specification this invention has been described in relation to certain preferred embodiments thereof, and many details have been set forth for purpose of illustration, it will be apparent to those skilled in the art that the invention is susceptible to alteration and that certain other details described herein can vary considerably without departing from the basic principles of the invention.

WHAT IS CLAIMED IS:

1  
2  
3  
4  
5  
6  
7  
8  
9  
10  
11  
12  
13  
14  
15  
16  
17  
18  
19  
20  
21  
22  
23  
24  
25  
26  
27  
28  
29  
30  
31

1. A multi-scale finite-volume method for use in modeling a subsurface reservoir comprising:
  - (a) creating a fine grid defining a plurality of fine cells and having a permeability field associated with the fine cells;
  - (b) creating a coarse grid defining a plurality of coarse cells having interfaces between the coarse cells, the coarse cells being aggregates of the fine cells;
  - (c) creating a dual coarse grid defining a plurality of dual coarse control volumes, the dual coarse control volumes being aggregates of the fine cells and having boundaries bounding the dual coarse control volumes;
  - (d) calculating dual basis functions on the dual coarse control volumes by solving local elliptic or parabolic problems;
  - (e) extracting fluxes across the interfaces of the coarse cells from the dual basis functions;
  - (f) assembling the fluxes to calculate effective transmissibilities between coarse cells;
  - (g) calculating pressure in the coarse cells using a finite volume method and utilizing the effective transmissibilities between coarse cells; and
  - (h) computing a fine-scale velocity field.

- 1    2.    The method of claim 1 wherein:  
2  
3        the fine-scale velocity field is computed directly in place.  
4
- 5    3.    The method of claim 2 wherein:  
6  
7        the step of computing a fine-scale velocity field directly in place  
8        includes:  
9
- 10        (i)    computing fine-scale fluxes across the coarse cell interfaces  
11            using the dual basis functions with the pressures the coarse  
12            cells;  
13
- 14        (ii)   solving a pressure equation on each of the coarse cells using  
15            the fine-scale fluxes computed in step (i) as boundary conditions  
16            to obtain fine-scale pressures; and  
17
- 18        (iii)   computing the fine-scale velocity field from Darcy's law using the  
19            fine-scale pressure obtained in step (ii).  
20
- 21    4.    The method of claim 3 wherein:  
22  
23        the solving of the pressure equation of step (ii) to obtain fine-scale  
24        pressures is performed on a system with larger support.  
25
- 26    5.    The method of claim 4 wherein:  
27  
28        the solving of the pressure equation of step (ii) may be performed by  
29        over-sampling around the coarse cells.

- 1 6. The method of claim 3 wherein:  
2  
3 the solving of the pressure equation of step (ii) may be performed by  
4 over-sampling around the coarse cells.

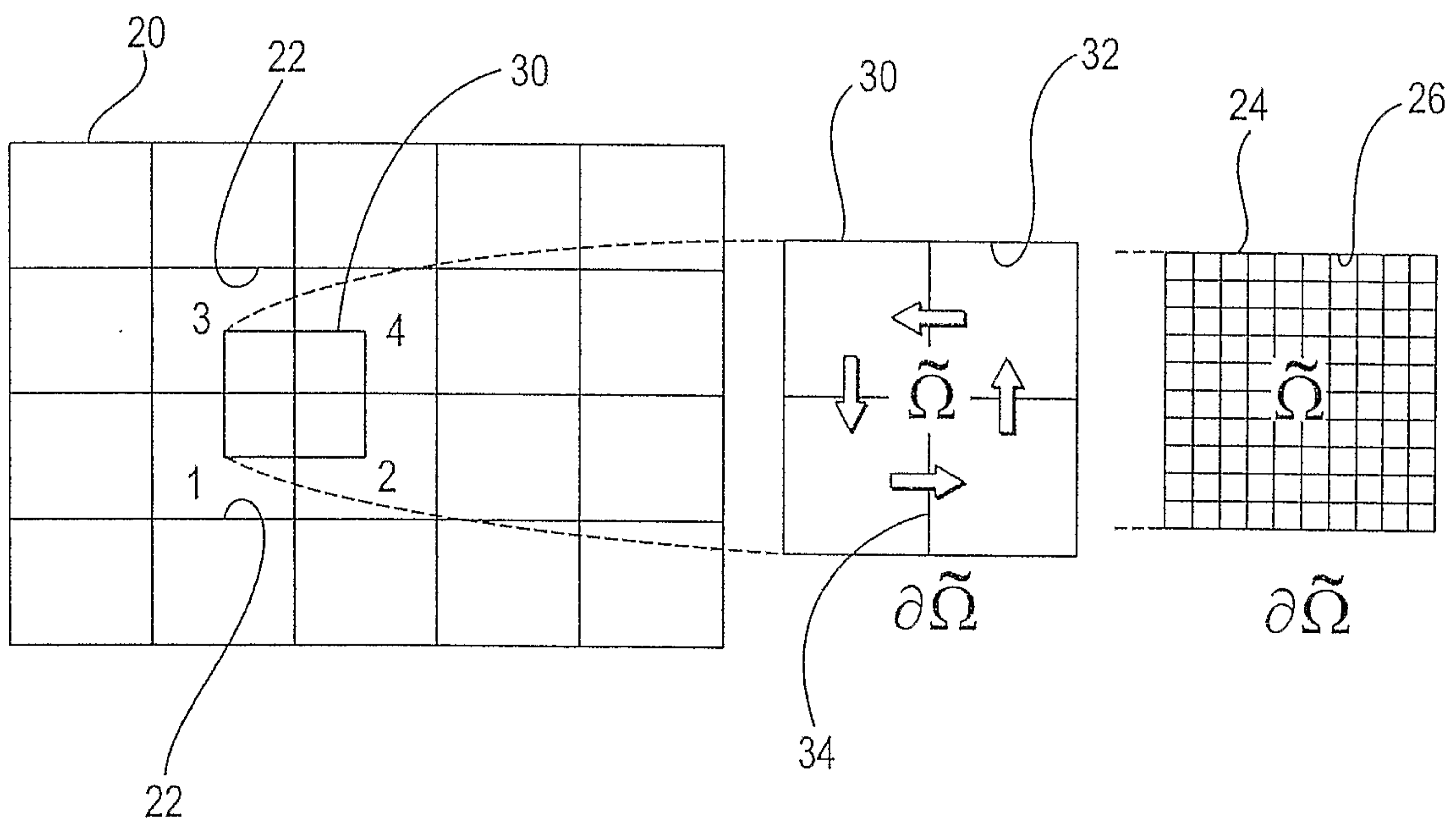


FIG. 1



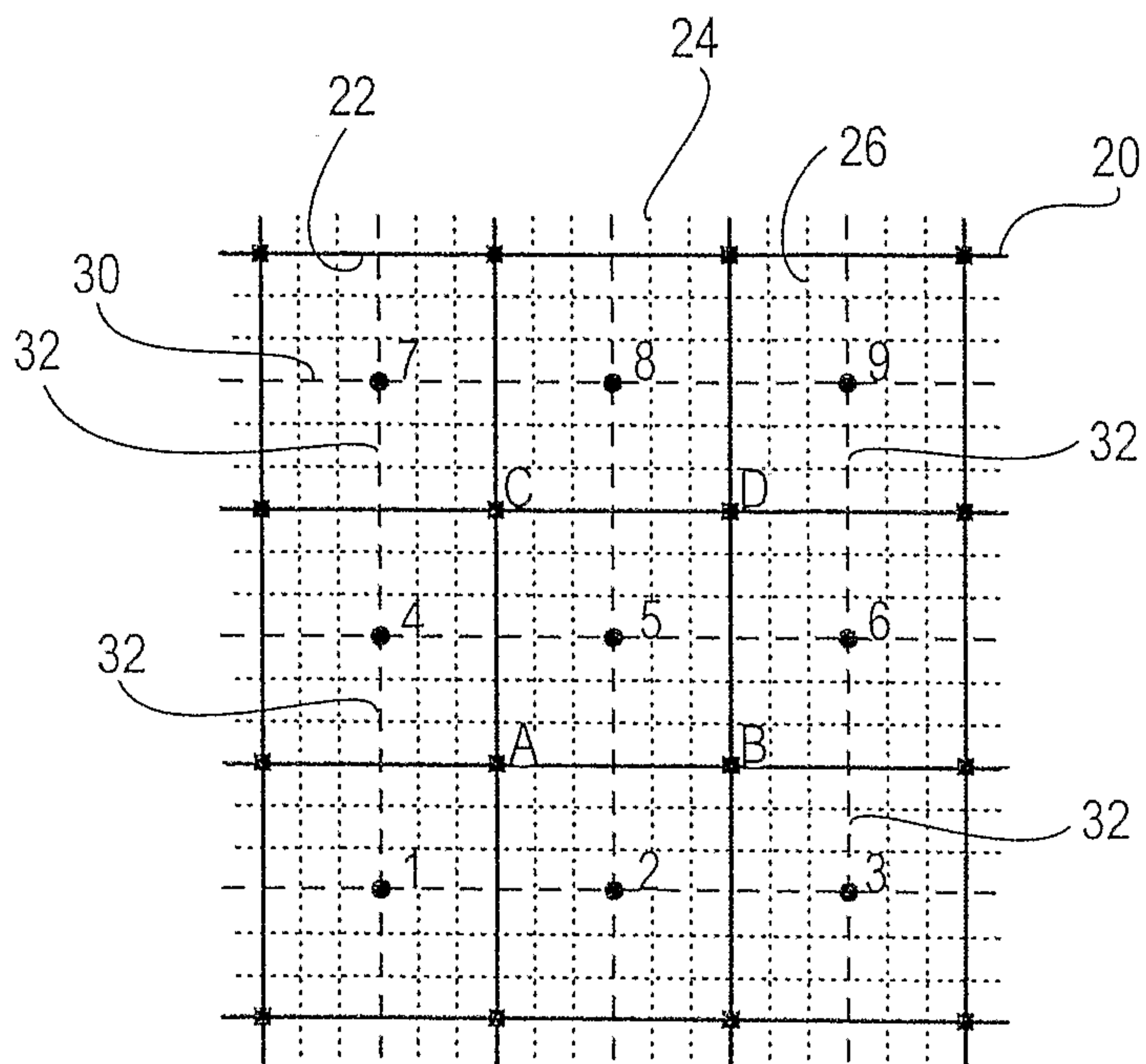


FIG. 2

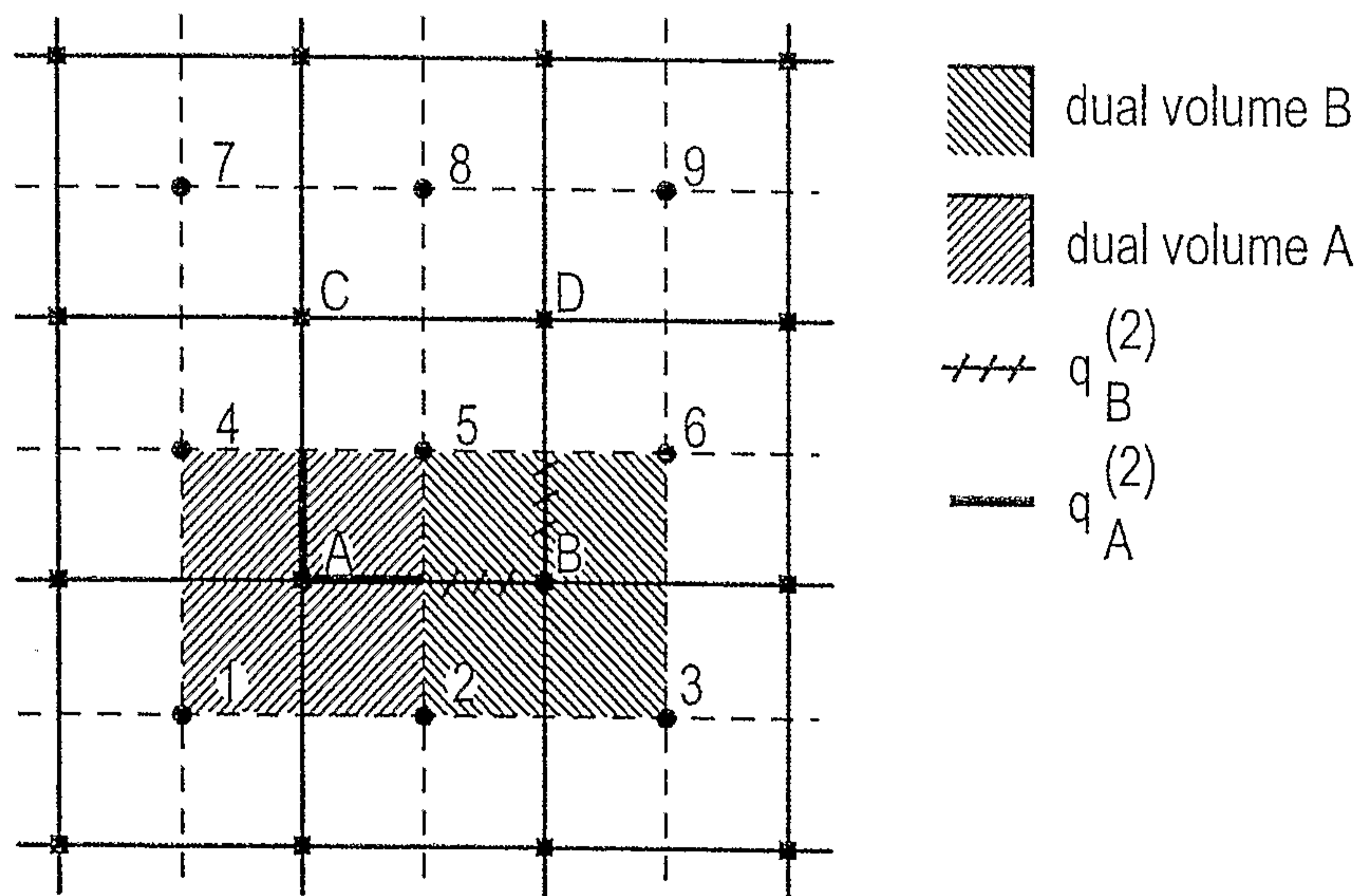


FIG. 3

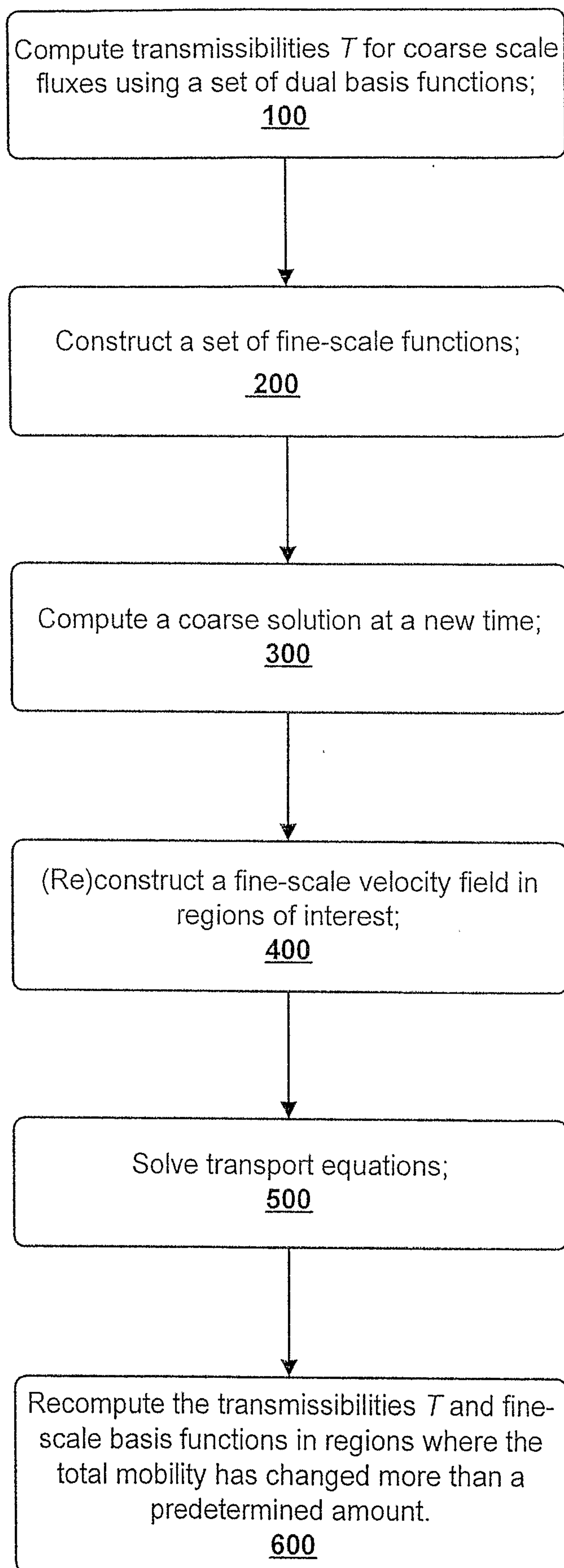
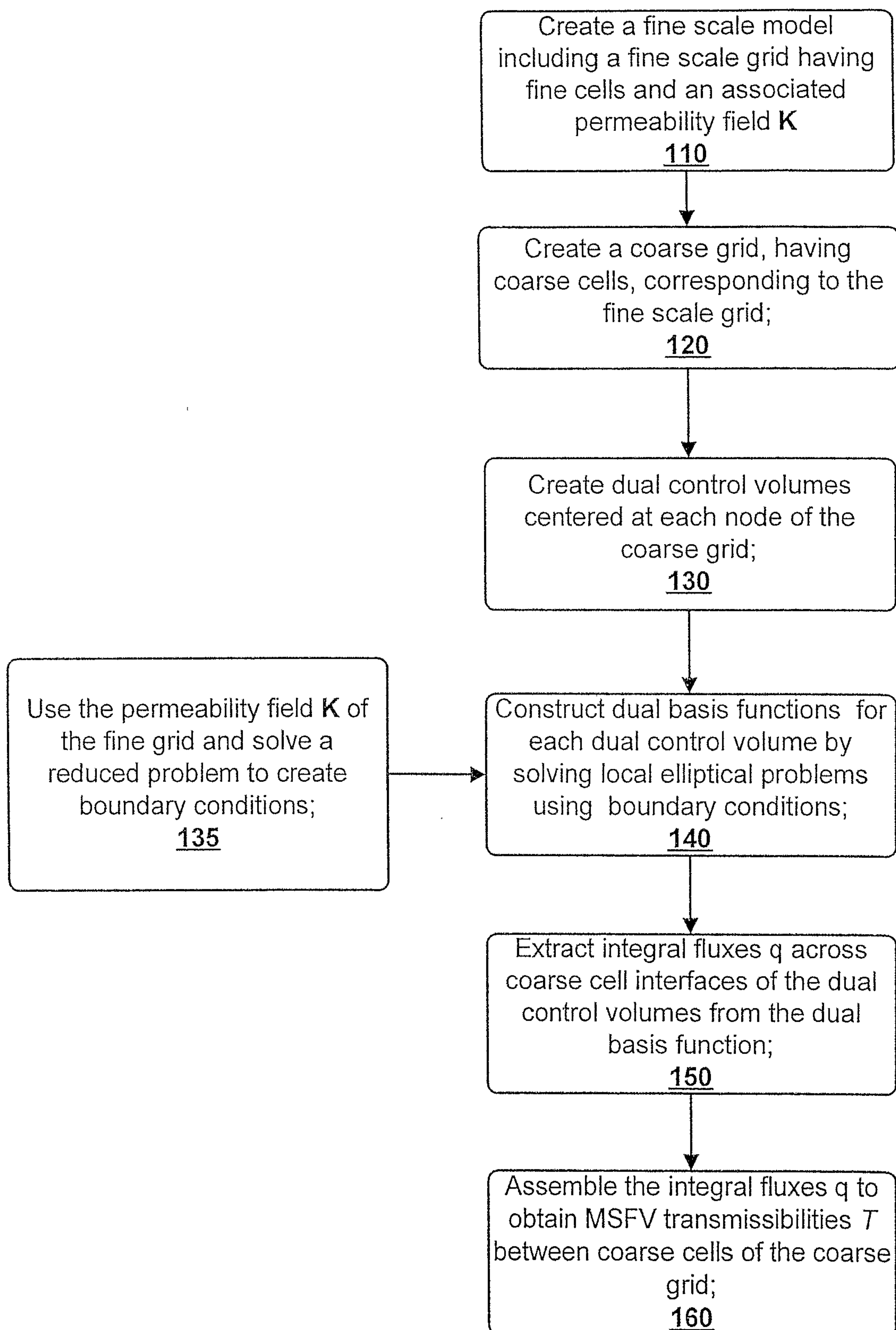


FIG. 4



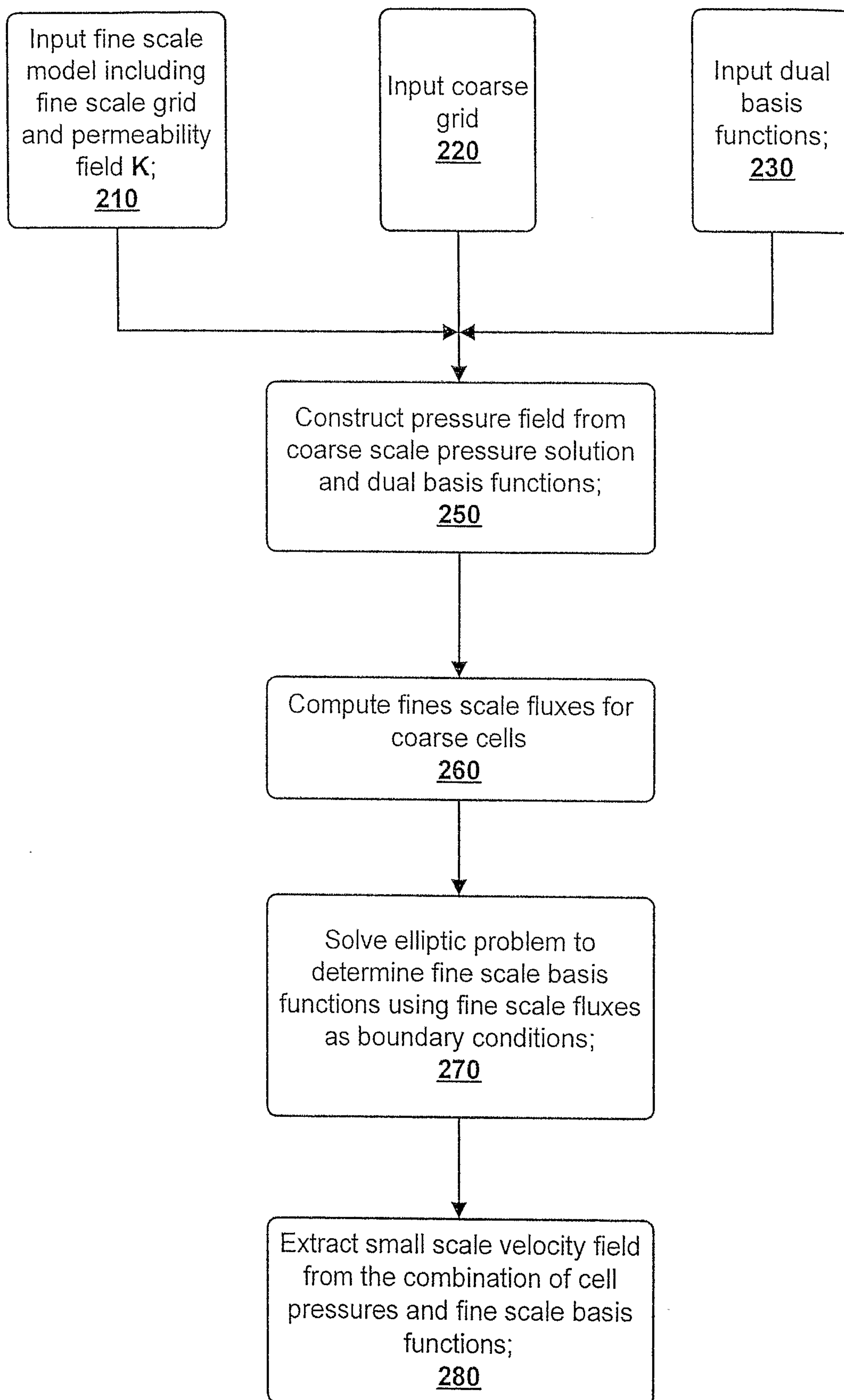


FIG. 6

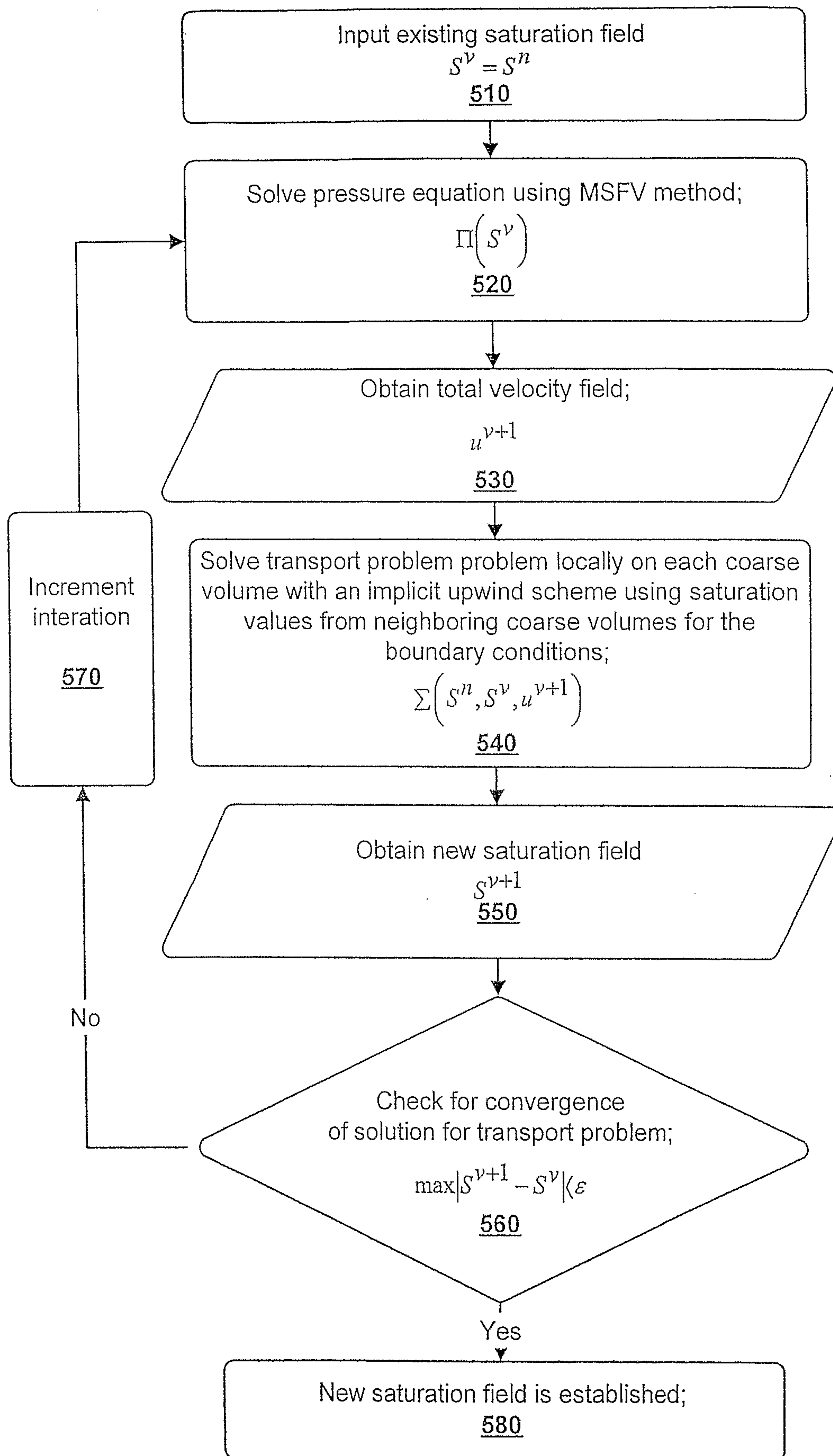


FIG. 7

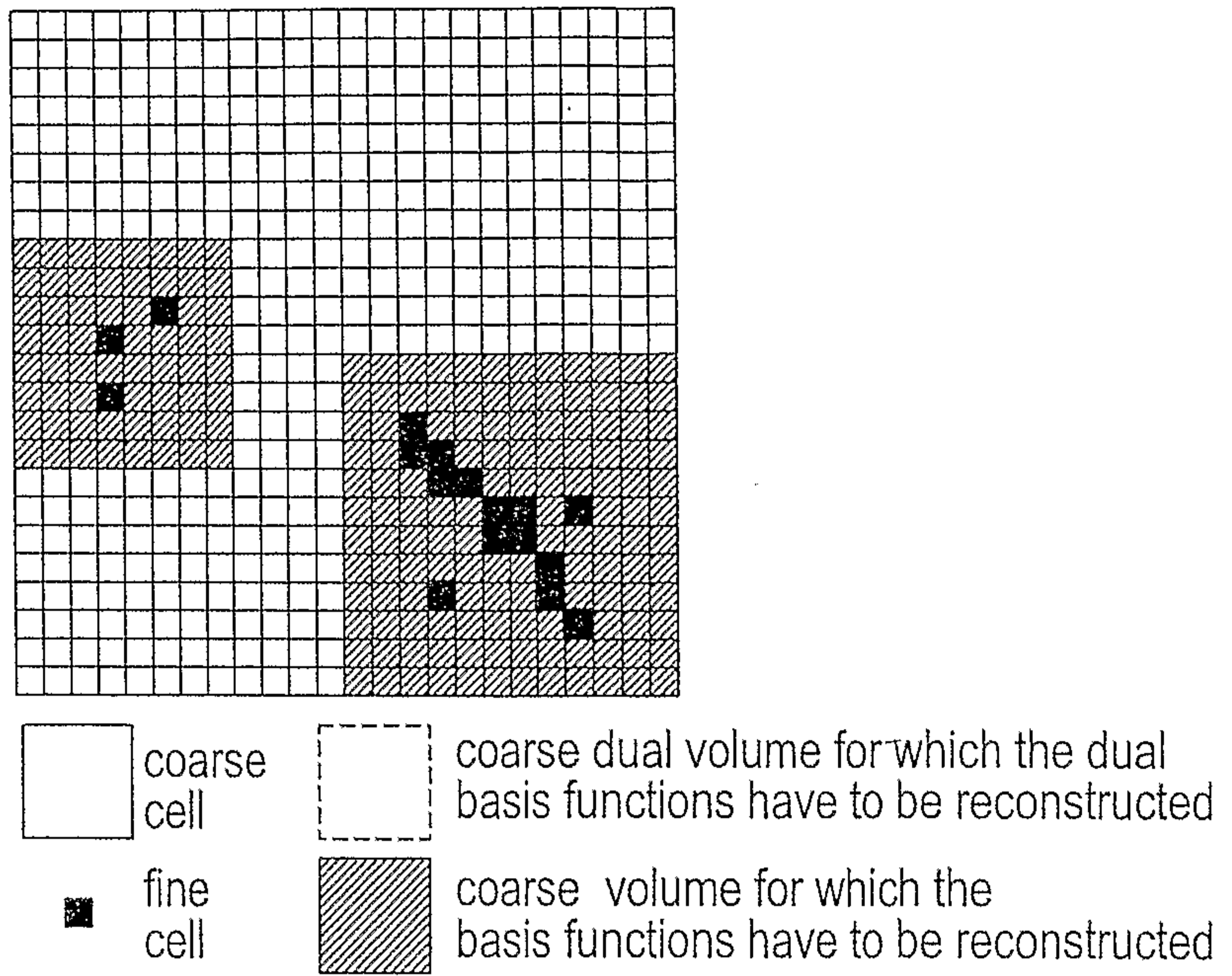


FIG. 8

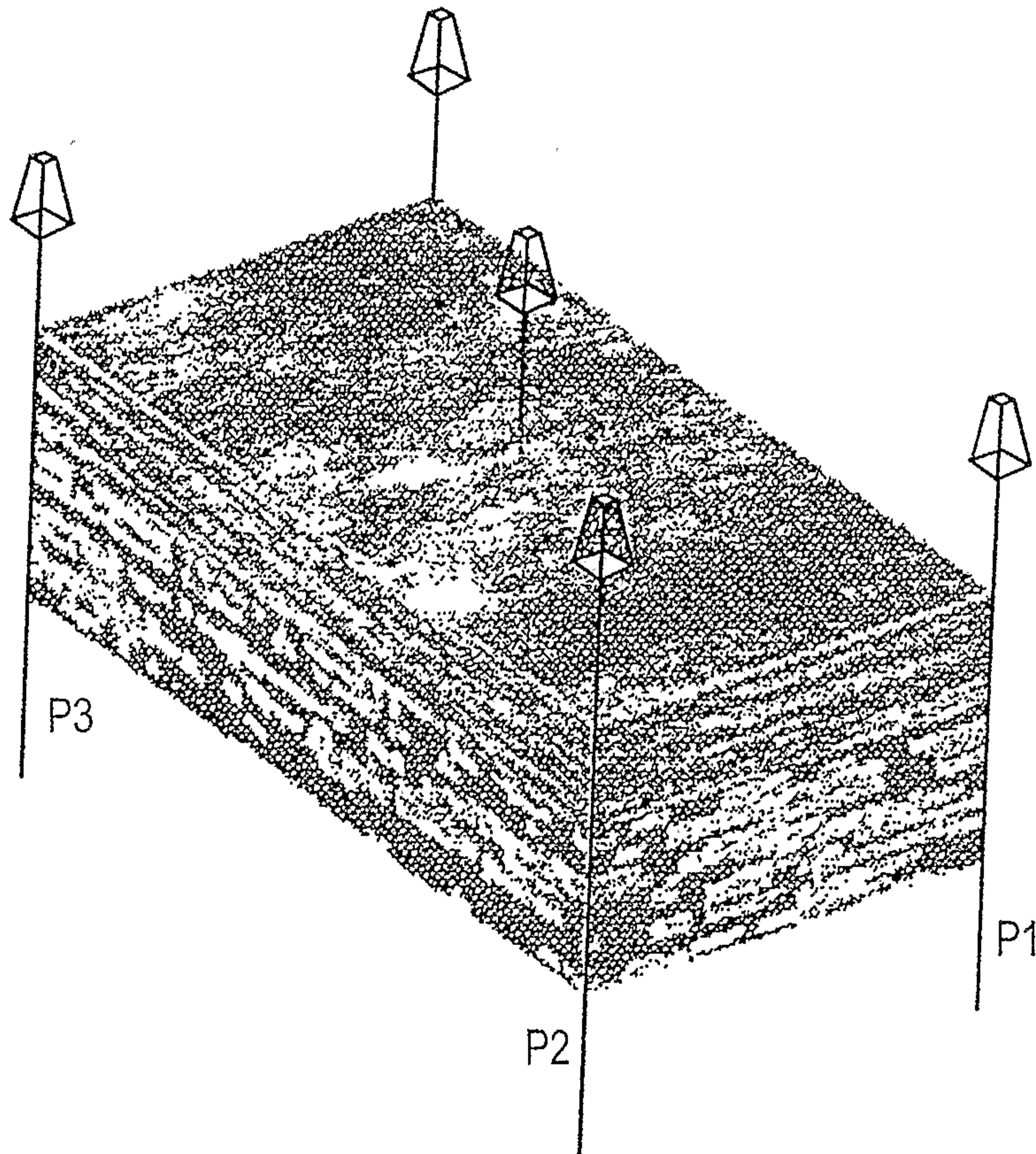


FIG. 9

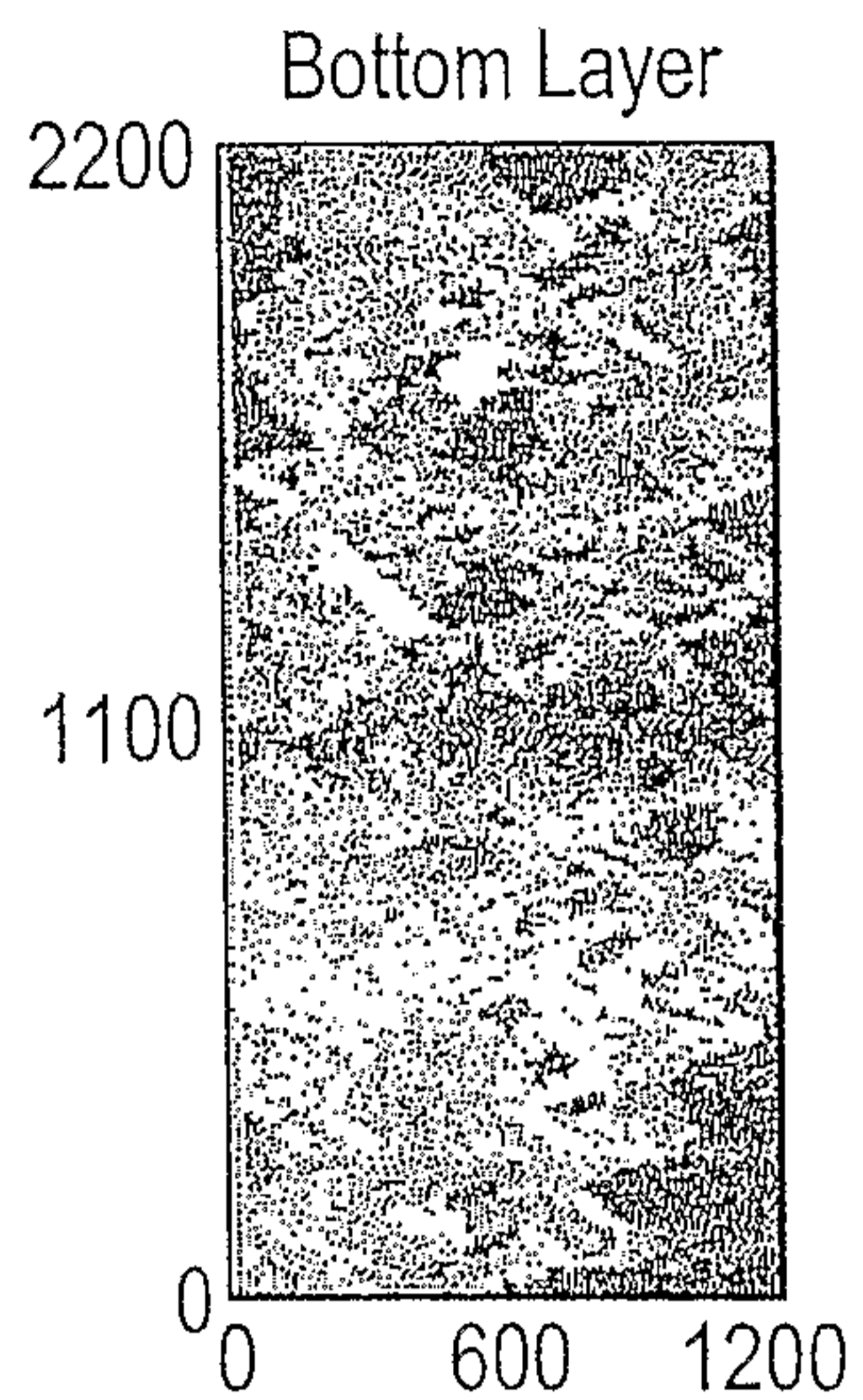


FIG. 10A

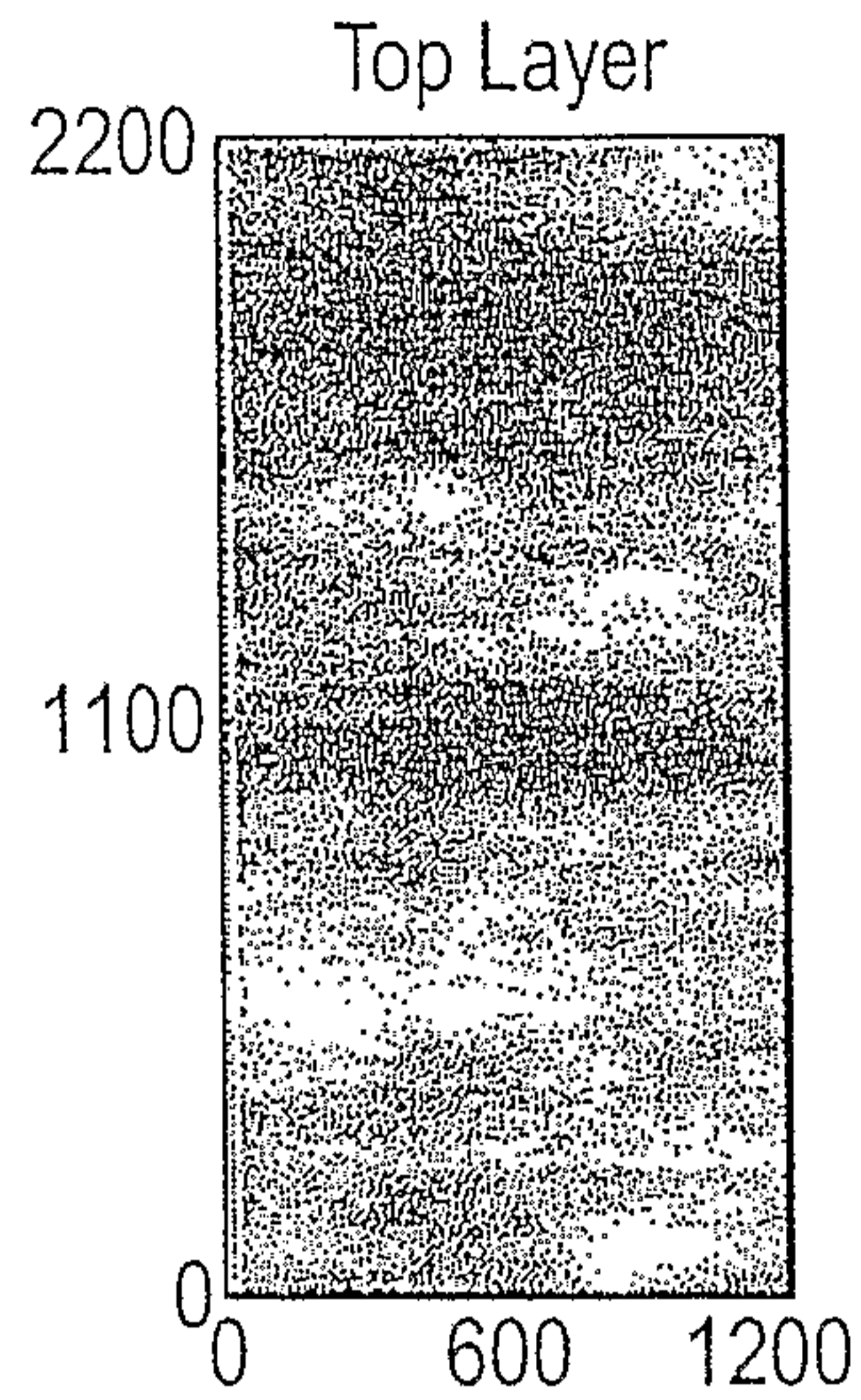


FIG. 10B

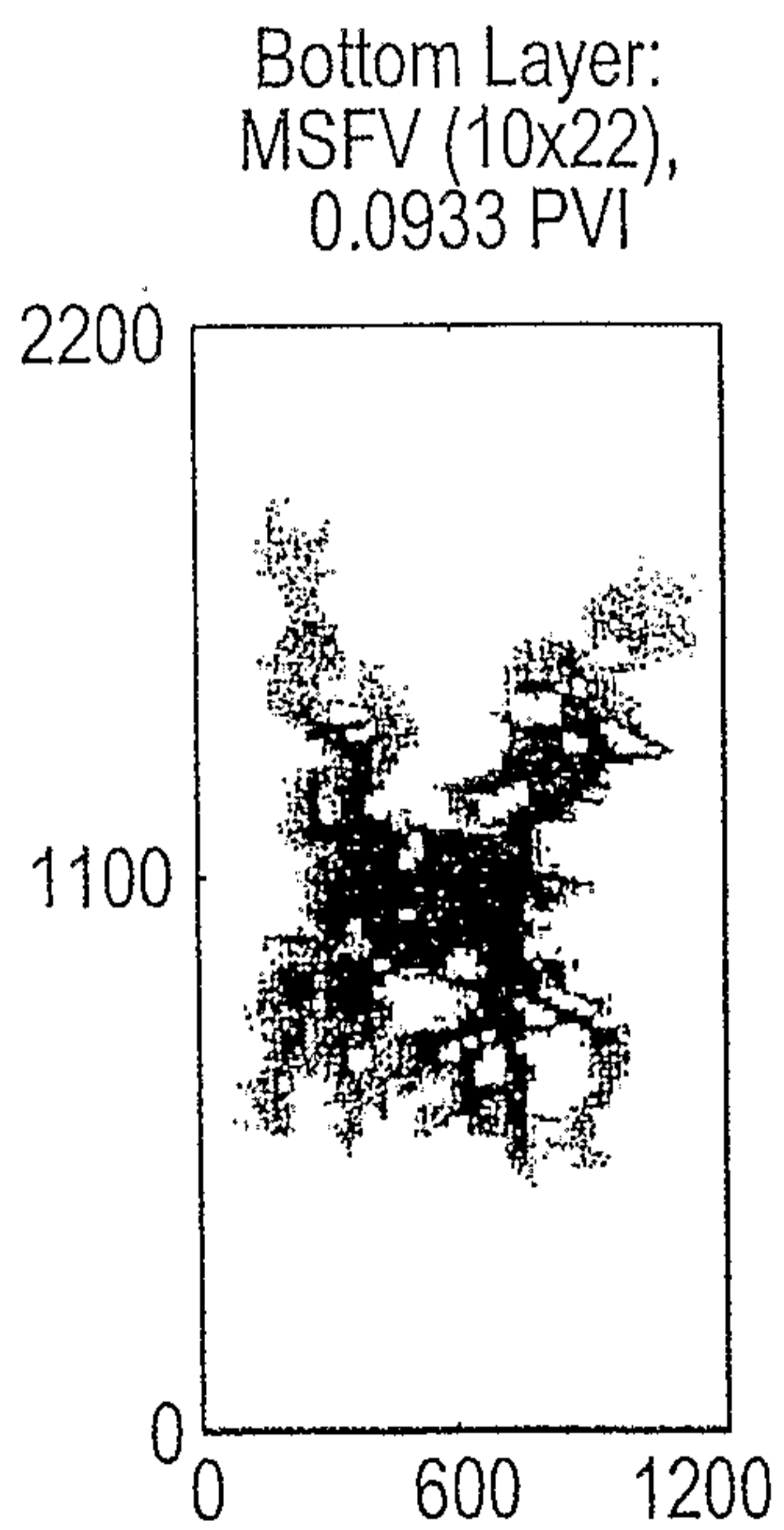


FIG. 11A

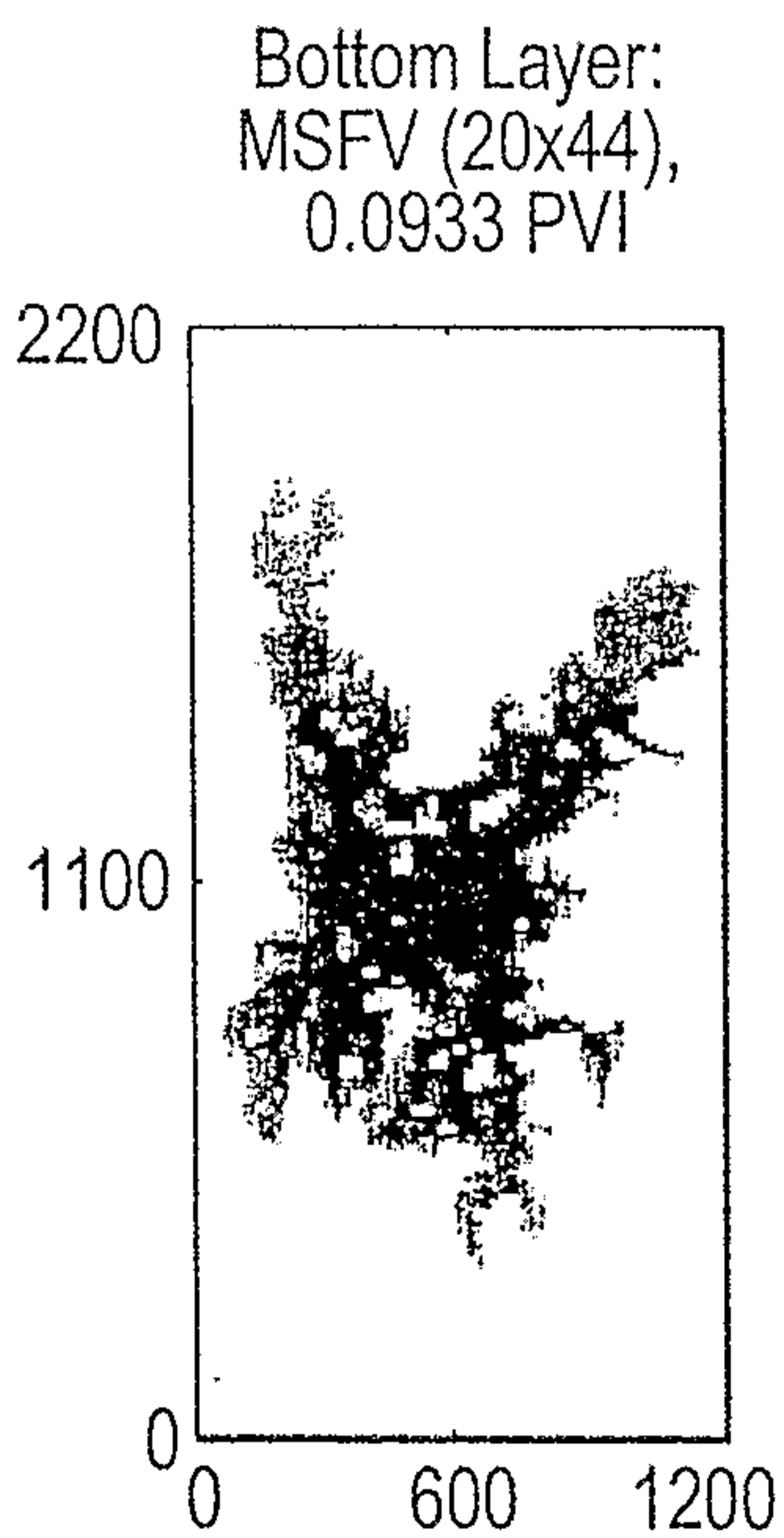


FIG. 11B

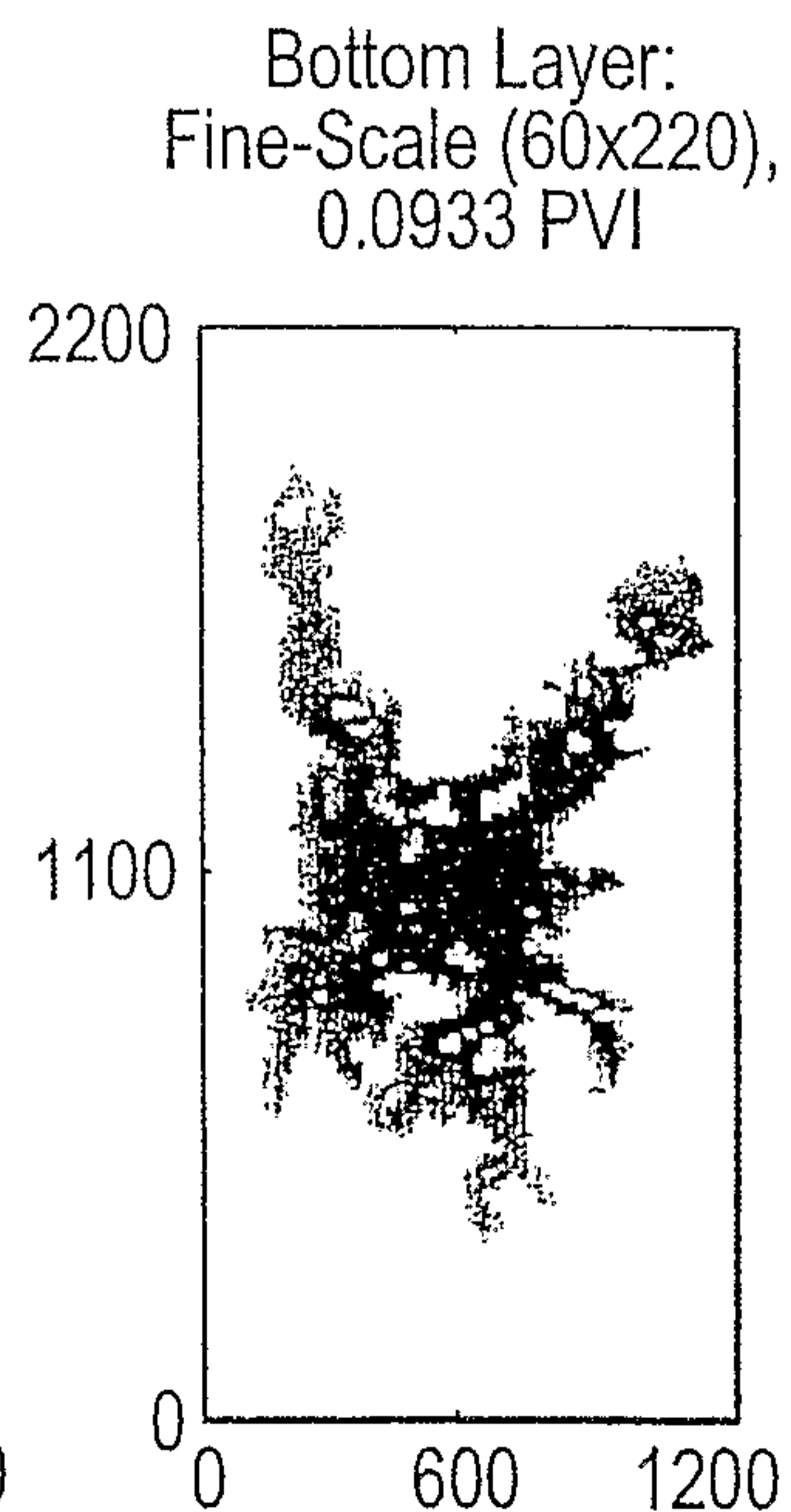


FIG. 11C

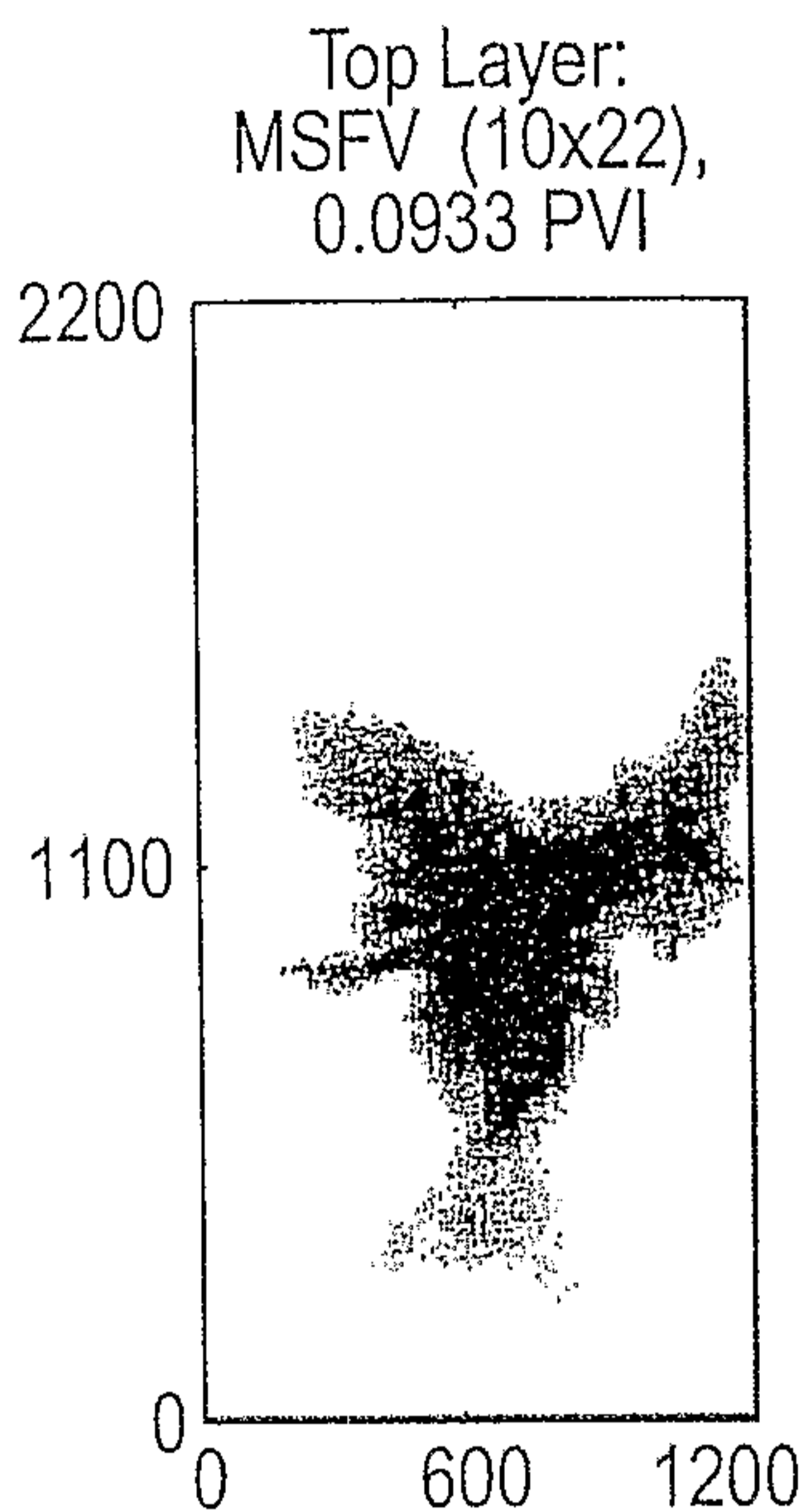


FIG. 12A

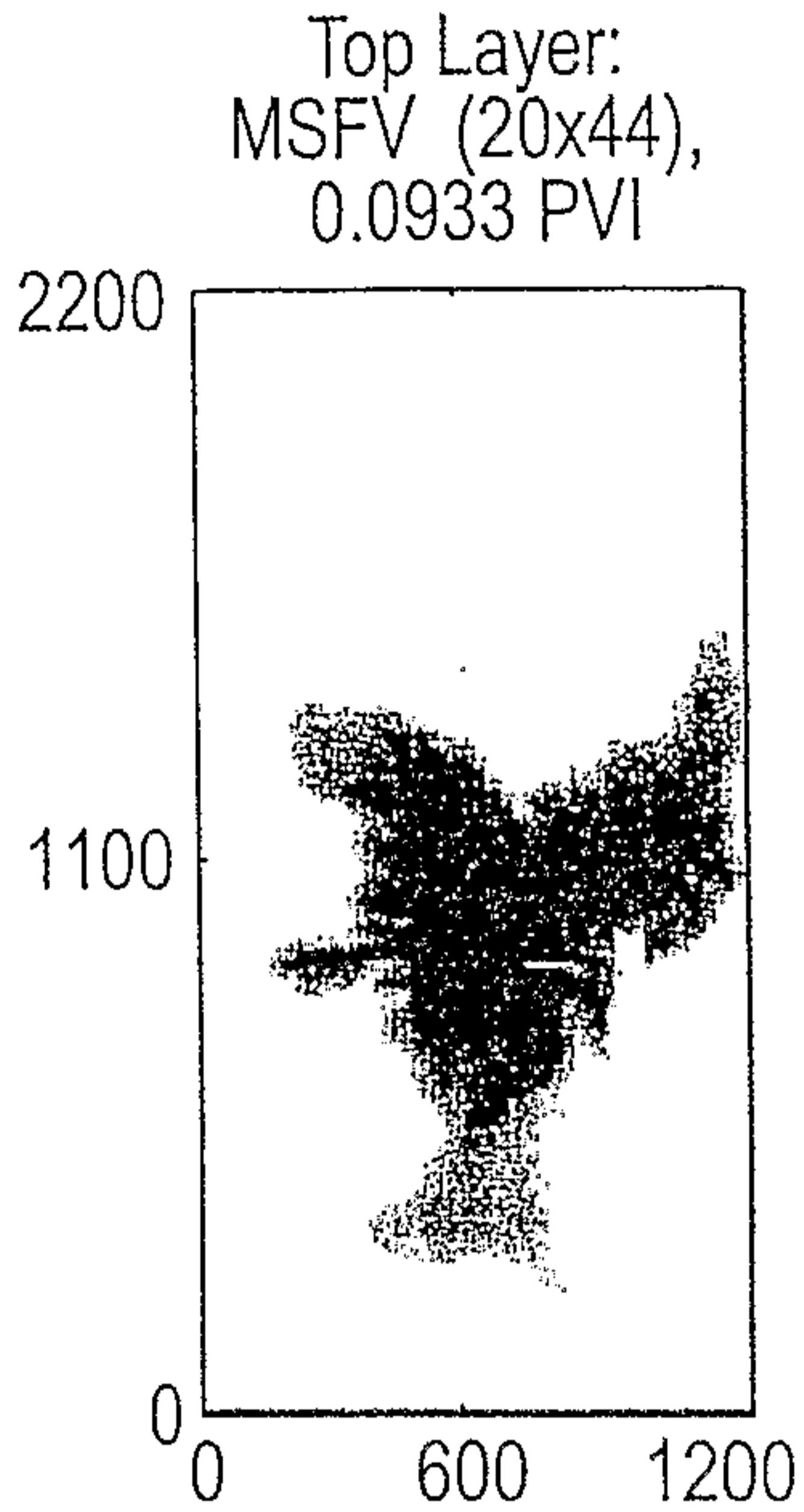


FIG. 12B

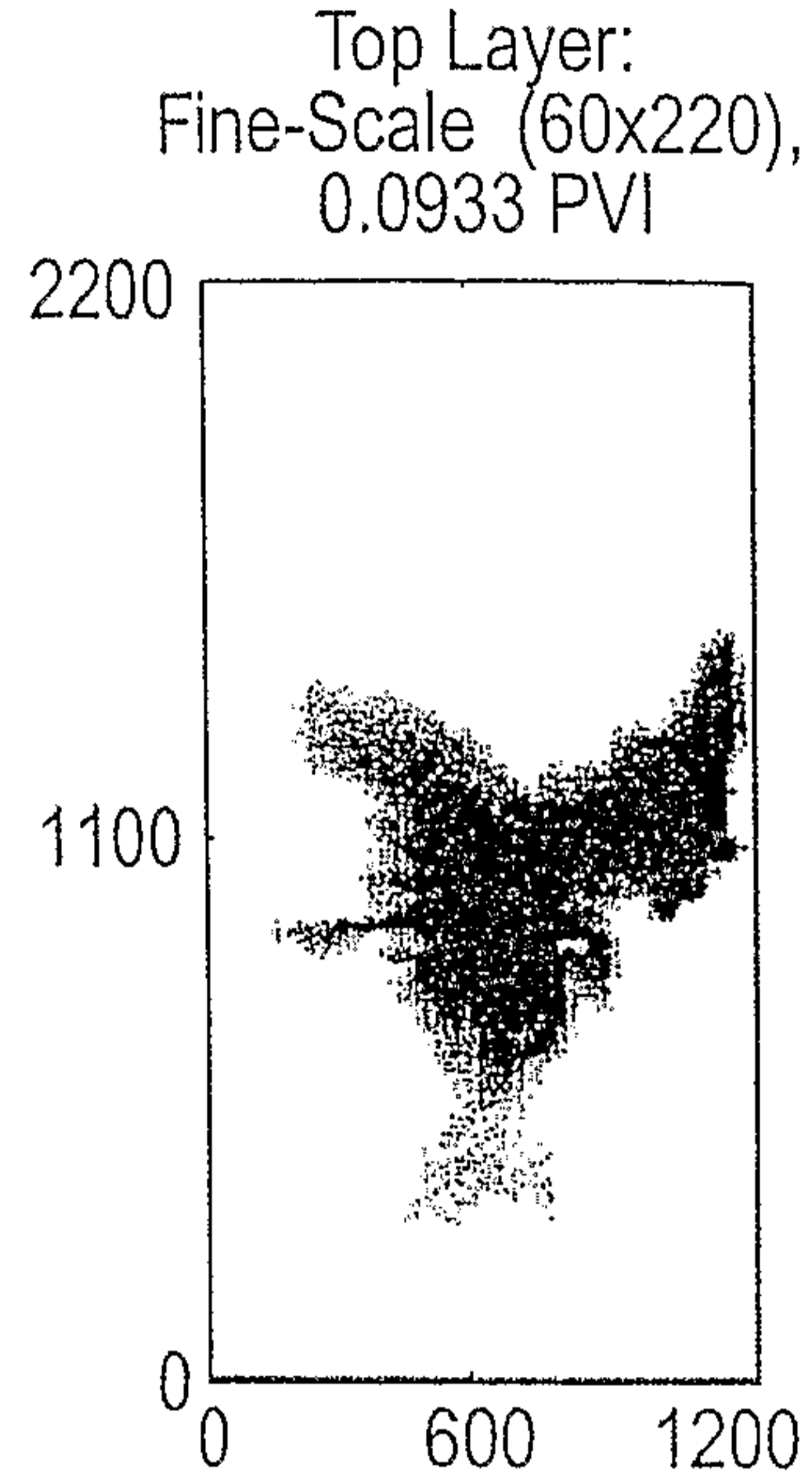


FIG. 12C

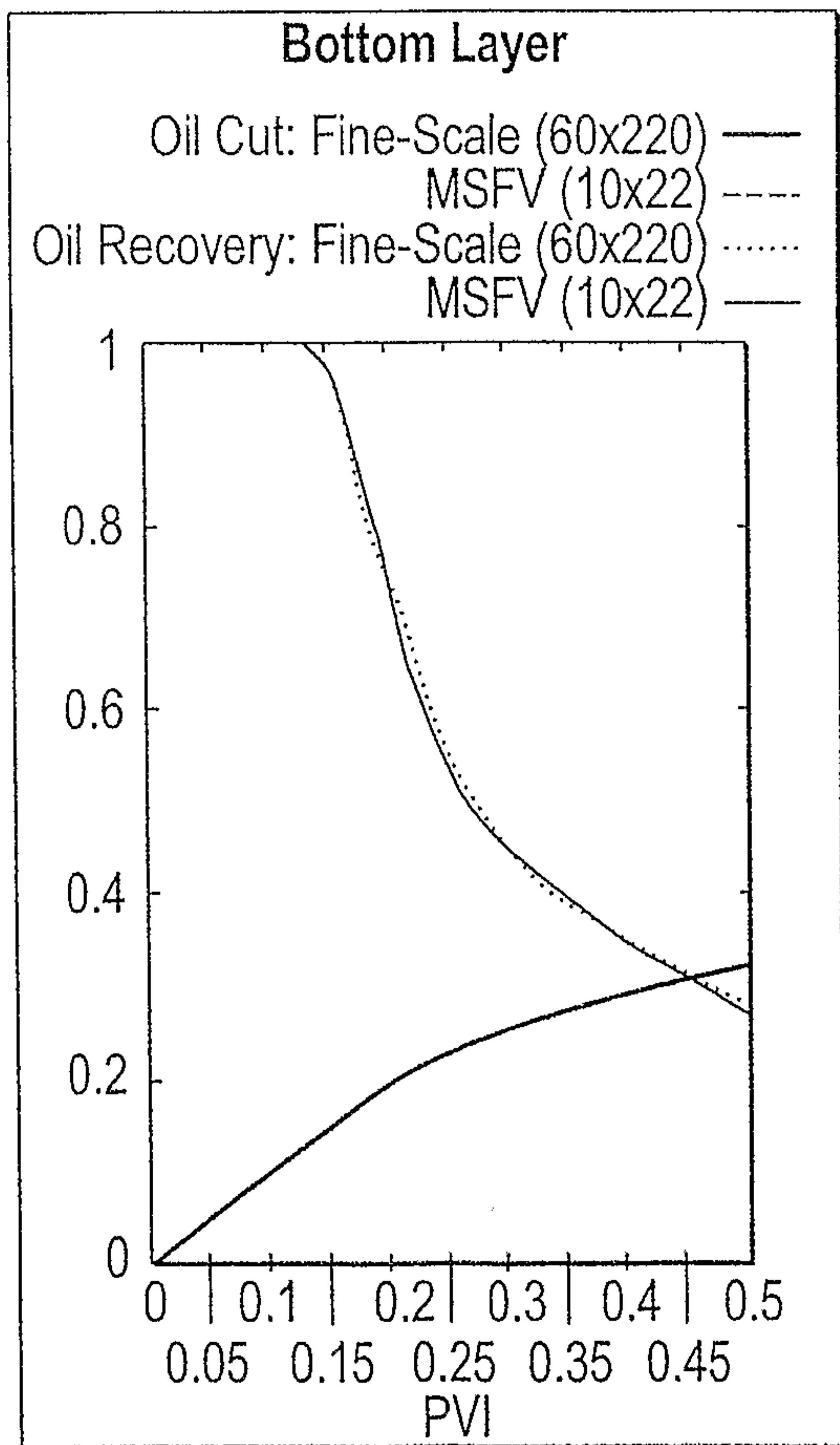


FIG. 13A

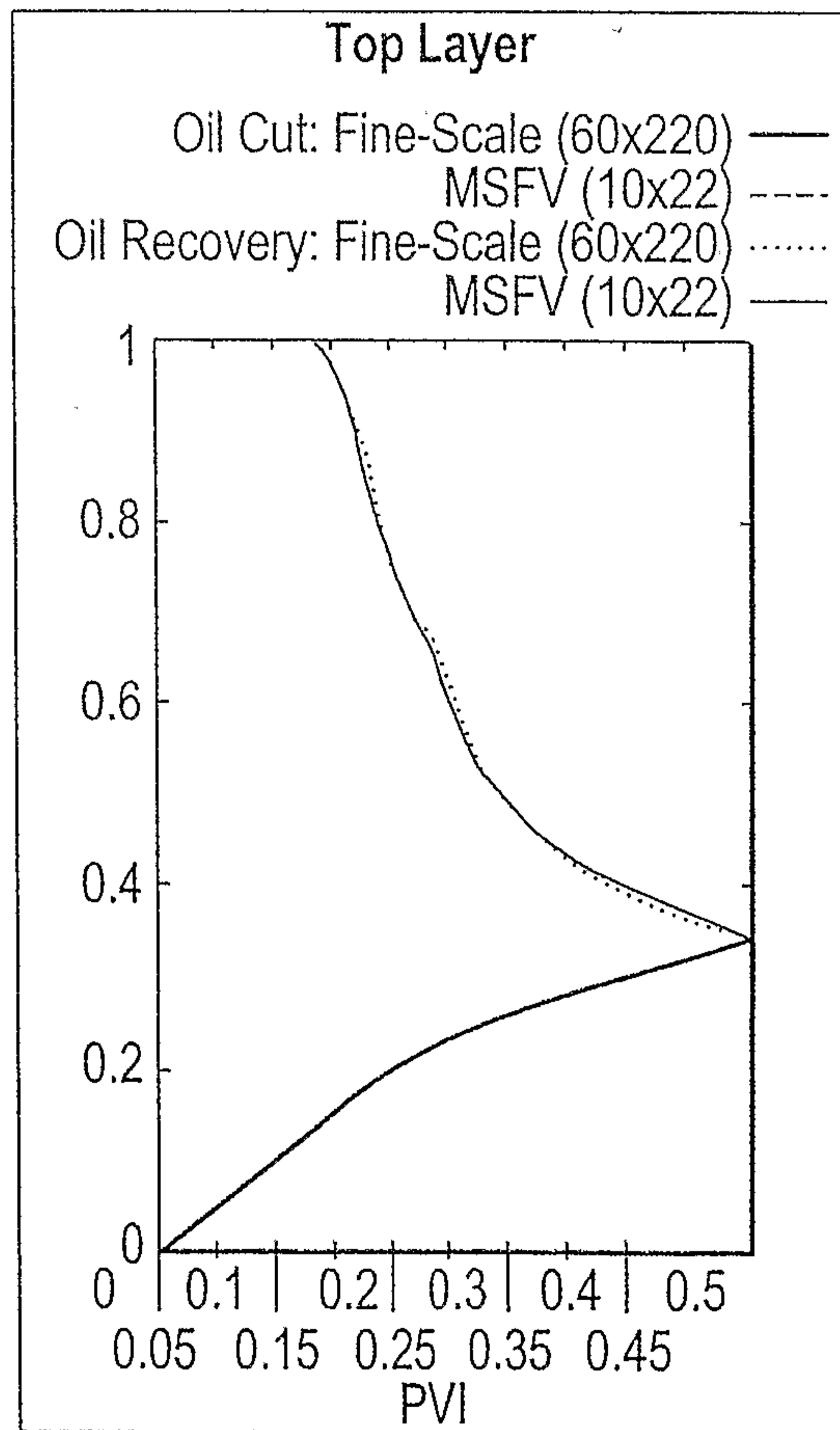


FIG. 13C



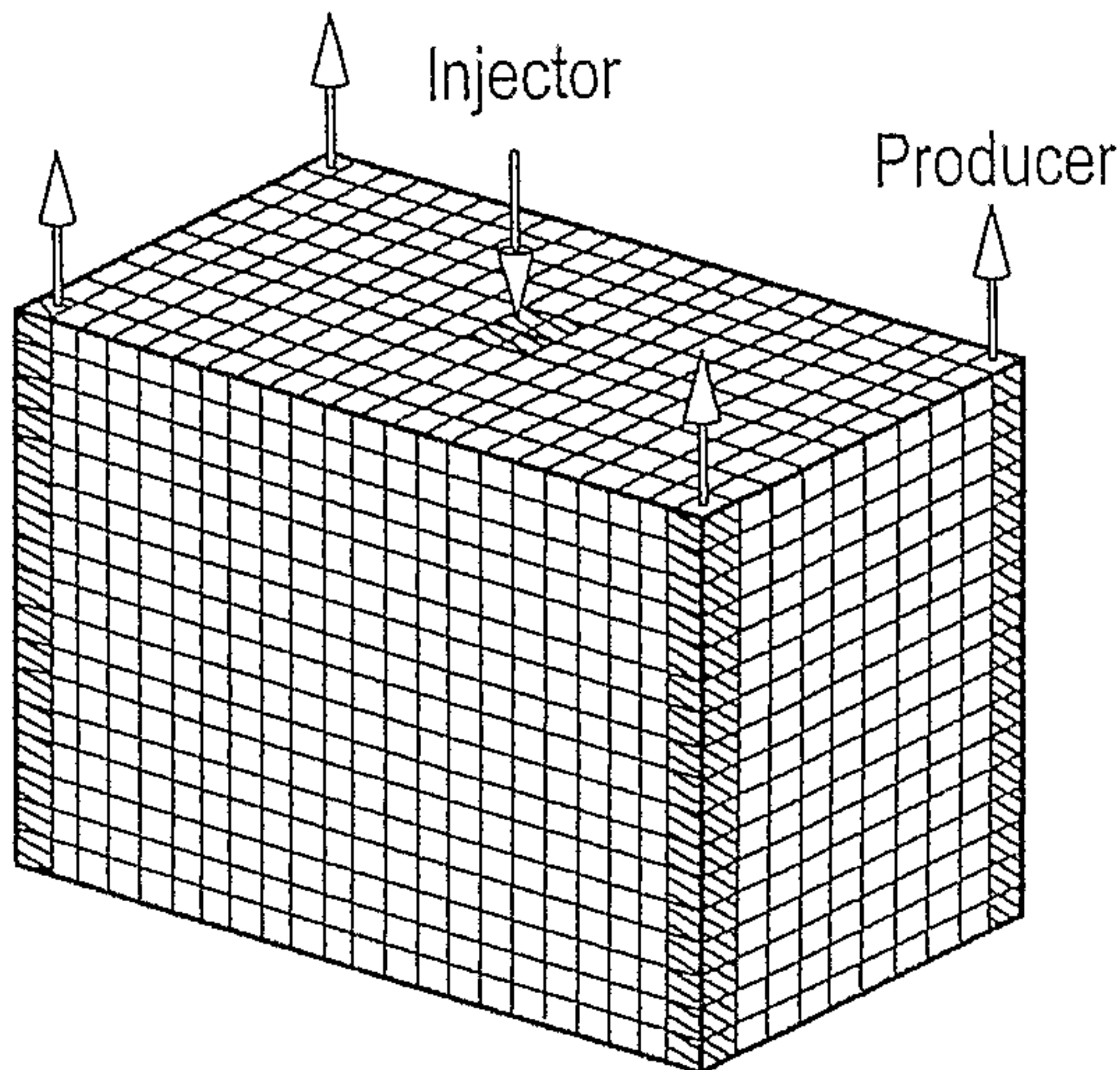


FIG. 14

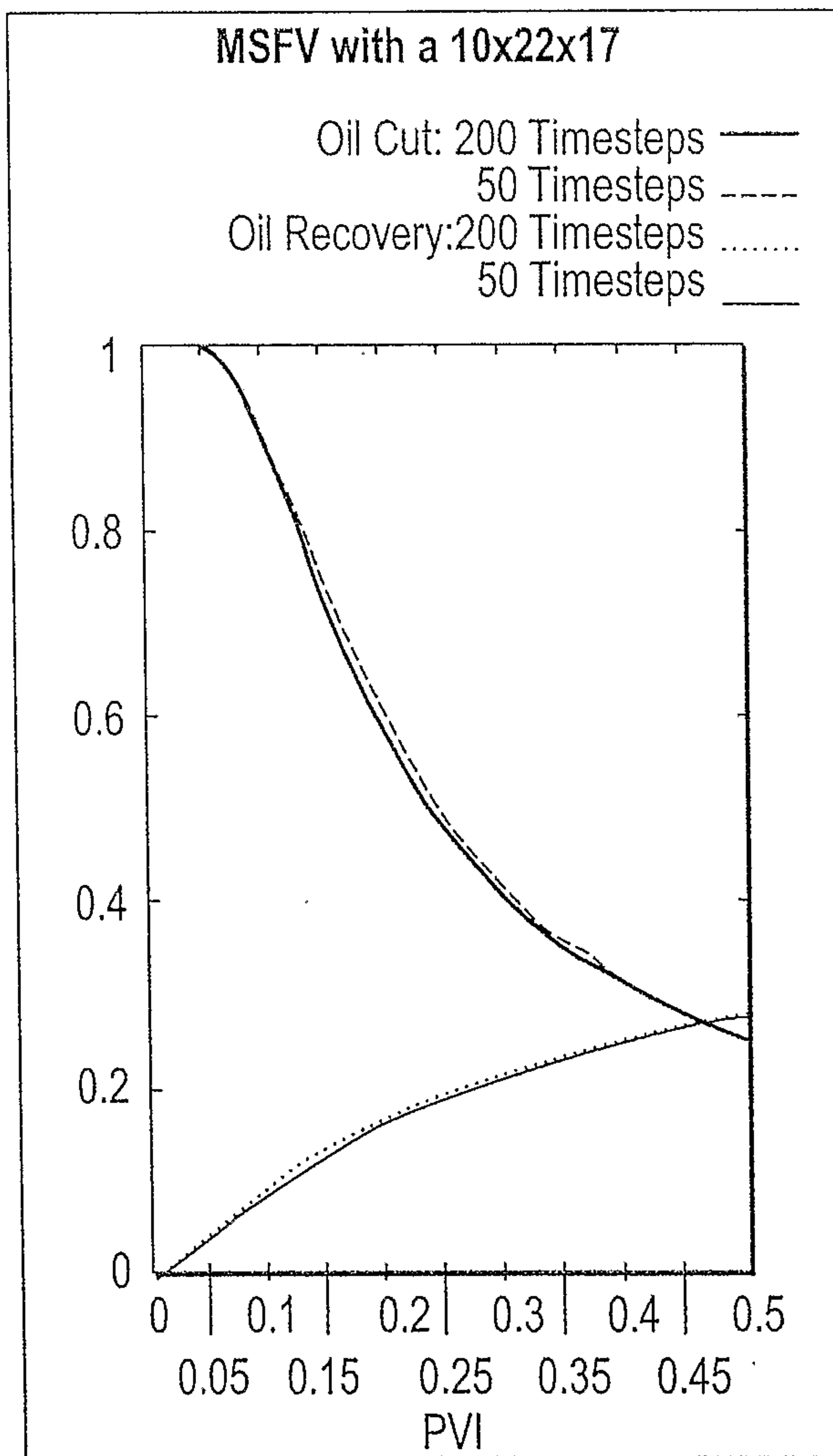


FIG. 15

